THE UNIVERSITY OF MICHIGAN

COLLEGE OF ENGINEERING
Department of Aeronautical and Astronautical Engineering
High Altitude Engineering Laboratory

Final Technical Report

# ATMOSPHERIC MEASUREMENTS OVER KWAJALEIN USING FALLING SPHERES

J. W. Peterson
W. H. Hansen
K. D. McWatters
G. Bonfanti

ORA Project 05436

under contract with:

DEPARTMENT OF THE NAVY, PACIFIC MISSILE RANGE
CONTRACT NO. N123(61756)31925A(PMR)
SCHEDULE NO. 30339
POINT MUGU, CALIFORNIA

administered through:

OFFICE OF RESEARCH ADMINISTRATION ANN ARBOR

January 1965

This report was prepared as a paper for the Journal of Geophysical Research.

TABLE OF CONTENTS


| | Page |
|---|---|
| ABSTRACT | 2 |
| INTRODUCTION | 3 |
| SYSTEM DESIGN | 3 |
| EXECUTION OF THE MEASUREMENTS | 7 |
| DATA ANALYSIS PROCEDURES | 12 |
| DRAG COEFFICIENTS | 22 |
| INTERPRETATION OF THE ATMOSPHERIC PROFILES | 25 |
| CONCLUSIONS | 31 |
| ACKNOWLEDGMENTS | 33 |
| REFERENCES | 34 |
| LIST OF TABLES | 37 |
| LIST OF FIGURES | 43 |

# ATMOSPHERIC MEASUREMENTS OVER KWAJALEIN USING FALLING SPHERES

J. W. Peterson, W. H. Hansen, K. D. McWatters, and G. Bonfanti

High Altitude Engineering Laboratory
Department of Aeronautical and Astronautical Engineering
The University of Michigan, Ann Arbor

## ABSTRACT

This paper presents and discusses the results of 13 firings over a 15-month period at Kwajalein. Inflatable spheres of mass 50 grams and diameter 66 cm were deployed from Nike-Cajun rockets on the ascending part of the trajectory and tracked by the Tradex radar. Density and temperature profiles were derived from the tracking data from as low as 32 km to as high as 120 km. Horizontal wind profiles were also derived to 70 km. Measured temperatures were higher than the U. S. Standard, 1962 near 50 km and lower near 100 km. An indication of atmospheric heating was found in six of the profiles near 85 km. A day-night pair of soundings showed a relatively large increase in the daytime density that was not accompanied by a change in the temperature profile.

## INTRODUCTION

The falling sphere has been used in a number of configurations for air density measurement. Bartman et al. [1956] used a 1.2-meter inflated sphere of mass 22 kg and the Dovap system for tracking, which required a relatively heavy transponder. A later development was an 18-cm sphere with an internal accelerometer and telemeter whose total mass was 5 kg [Jones et al., 1959]. In this case the mass-to-area ratio was less favorable, but the sensitive accelerometer resulted in an increased altitude capability. A third configuration used an inflated 1-meter sphere of mass 0.1 kg tracked by the AN/FPS-16 radar [Peterson and McWatters, 1964]. A further increase in altitude capability was achieved due to the very light weight of the sphere. These three systems were reported by The University of Michigan.

Falling spheres have been used by other investigators, among them Faucher et al. [1963], who measured air density above 100 km with a 2.74-meter inflated sphere whose mass, including accelerometers and telemeters, was 13 kg. The Robin, a 1-meter 115-gram sphere, has been used in large numbers with the Arcas rocket, whose peak altitude is approximately 70 km [Leviton and Wright, 1961; Lenhard, 1963].

## SYSTEM DESIGN

The present falling-sphere system was designed to meet the requirements of the Pacific Missile Range. The primary objective of the Kwajalein firings

was to measure, with an accuracy of 5% if possible, air density from about 30 km, where rawinsondes can be used, to 100 km. The measurement of wind in the atmosphere was a second objective.

A good quality radar at Kwajalein, the Tradex (Figure 1), suggested the use of falling spheres tracked by radar. No accelerometers or telemetering equipment were required since the desired atmospheric parameters could be found by processing radar-tracking data. Acceleration can be determined more accurately with an accelerometer than with tracking data. This factor, however, is offset by the very light weight of the spheres that can be used when instrumentation is not carried in the sphere.

The Nike-Cajun rocket (Figure 2) was selected because it could provide the desired altitude and velocity. The Nike-Cajun can carry a larger payload than was needed for this mission. A smaller rocket could have been used had one with proven reliability been available at the time. A rocket of higher performance than the Nike-Cajun would increase the altitude limit of the measurement very little. More speed would, however, increase the accuracy of drag-coefficient calculations at very high altitude. On the other hand, the aerodynamic heating experienced by the sphere is significant. The use of a higher performance rocket might result in heat failure of the sphere envelope.

The spheres were made as light as possible in order to increase the sensitivity of the system to atmospheric density and wind shear. Spheres made of the polyester material Mylar of half-mil thickness (0.0125 mm) were inflated with isopentane gas released from a capsule carried in the sphere. When fully inflated, each sphere was checked by measurements on six different

diameters. The difference between maximum and minimum diameters was typically 0.5 per cent and never more than 1.0 per cent. The weight breakdown was approximately: envelope material, 34 grams; isopentane, 8 grams; and capsule, 8 grams. Since the envelope material constituted most of the weight, its thickness was a critical factor. It was thought that a thinner material would be too vulnerable to the abuse sustained when packed and when deployed. Thinner material is also more permeable. The behavior of falling spheres is governed primarily by the ratio of mass to area. If all the mass is in the surface, the ratio depends on the density of the envelope material and its thickness, and is independent of sphere diameter. In this design the sphere diameter was not an important factor. Due to the power of Tradex, almost any sphere diameter would provide adequate reflecting surface. The sphere of 66-cm diameter which was used lies in a good range for drag-coefficient data and can easily be packed in the available space. Mylar, metalized on the outer surface, with a surface resistance of approximately 1 ohm per square was used to increase the reflectivity of the sphere envelope as a radar target. A three-sphere payload (Figure 3) was used because sphere deployment and inflation problems were anticipated. The second and third spheres added nothing to the measurement capability of the system but provided alternate targets for the radar if the first sphere failed. Each sphere was packed between a pair of plastic staves in a cylindrical space of length 28 cm and diameter 2.5 cm. The available volume was 141 cc, the capsule volume was 20 cc, and the volume of envelope material was 22 cc. Sphere and staves were ejected through the end of the tube at approximately 30 meters per second by 3/4 gram of black powder.

The ejections were timed by a three-switch Raymond timer (Figure 4). The timer was started by rocket motion off the launcher. Each ejection could be set at an arbitrary time up to a maximum of 180 seconds, at which time the Cajun is near apogee and ascending.

Spheres were ejected in an aft direction (Figure 3) so that both aerodynamic drag and ejection velocity of the first sphere increased separation between sphere and rocket. It was believed that aft ejection would enable the radar to transfer from the rocket track to the sphere track in the shortest time.

The isopentane capsules on the first two flights were opened by pneumatic pressure. On all subsequent flights a more reliable, inertia-operated capsule was used (Figure 5). The acceleration of ejection, which is several hundred g's, deflects the prong, which is restrained by a spring, until the thin diaphragm is pierced, releasing isopentane. Sufficient isopentane was used to keep the spheres inflated at the 30-km level.

Geometrical considerations made the ascending portion of the trajectory the most favorable for sensitive density measurements at high altitude. At Kwajalein, more specifically, Roi-Namur Island, the radar site and launch pad were only about one mile apart. On ascent, therefore, azimuth and elevation angles were nearly stationary, and errors associated with the angles and angle rates were much smaller than during descent. Consequently, the precision of range and range rate became the factors limiting system sensitivity. Since Tradex can measure range rate as well as range with good precision it is well suited to high-altitude measurements. The ejection of the first sphere was set

for 70 seconds, when the rocket was expected to be at 85 km altitude. This was the earliest feasible ejection because the trajectory of the light-weight spheres would be greatly influenced by drag at lower levels and would fail to reach the desired altitude. Normal apogees for first sphere and Cajun were approximately 150 km and 180 km respectively (Table 1 and Figure 6).

It was anticipated that the altitude of the rocket at the time of first sphere ejection would be quite critical and should be controlled as accurately as possible. The time of Cajun ignition was believed to be the most important factor governing the altitude versus time function of the rocket. The ignition time, nominally 20 seconds, was determined by a delay squib whose delay time was not as precise as might be desired. All igniters were taken from the same manufacturer's lot in the hope that any variations due to unknown or uncontrollable factors in the manufacturing process would be minimized. Direct observations of ignition were difficult because radar tracks of this part of the trajectory were not obtained, and cloud cover often made visual observation impossible. The resulting sphere trajectories were an indirect indication of time of ignition; all fell within desirable limits except for the eighth firing, where the sphere apogee was relatively low. The first firing was also abnormal, but for other reasons.

## EXECUTION OF THE MEASUREMENTS

The first four firings were conducted by University of Michigan engineers in order to develop and test the system. Launch operations were carried out by New Mexico State University personnel, who were previously engaged in

similar firings at Kwajalein. Radar operations and data processing were carried out by Lincoln Laboratory and RCA personnel associated with the Press program. Computer programs for data processing were developed by the Michigan group. The fifth and subsequent firings were conducted by the personnel based at Kwajalein. Rawinsonde measurements were obtained by the Pacific Missile Range Weather Station, Kwajalein.

Sixteen firings were carried out in 1963 and 1964. Table 1 summarizes the results; Figure 6 shows a typical trajectory. Three shots failed to provide any atmospheric data; eleven were substantially successful. Ten shots resulted in a track on both ascent and descent.

The rockets were launched at quadrant elevation 85° and azimuth 320° approximately. The azimuth of the launch pad as seen from the Tradex was 275°. The Cajun was acquired by pointing the radar antenna at the intercept coordinates where the Cajun was expected to appear 33 seconds after launch. At this time the Nike booster was separated and Cajun thrusting was finished. The elevation angle of the radar antenna at intercept was 81°; the radar beam was 2°. In general this procedure was satisfactory except when the rocket failed to pass through the radar beam when expected. Failure to acquire resulted in loss of data on shots nine and ten. Only a small amount of data was recovered from shots five and six when acquisition was delayed several minutes. Ascent data on shot eleven were lost when a track of the Cajun was not obtained and initial tracking of the first sphere occurred near apogee.

The radar tracking procedure was first to establish a track on the Cajun. When the first sphere was ejected, the radar track was transferred to the

sphere as quickly as possible. The second and third spheres were ejected at higher altitude where the air density was too small to be measured. The radar track was transferred to each of these spheres, and the radar operator then chose the best of these to track on descent. The descending sphere was tracked until the fluctuations of cross section indicated deflation. Sphere deflation normally occurred near 30 km, approximately 18 minutes after rocket launching. After several firings had established that sphere inflation was reliable, the tracking requirement was changed so that the first sphere was tracked continuously on descent as well as on ascent. Table 1 indicates which spheres were tracked during each shot. The changed procedure was adopted because one could then prove that the motion of the ascending sphere was not influenced by escaping gas.

We found it difficult to build a sphere which would present a uniform cross section to the radar. The spheres were constructed from twenty gore pieces and two pole pieces. Fluctuations of radar cross section were probably due to poor electrical conductivity at the seams. The radar automatic-gain control data presented many different patterns. Different rates of sphere rotation and different orientations of sphere axis and rotation axis may account for the variety. Cross-section fluctuations caused a tracking error on sounding 8 when the radar operator decided the first sphere had deflated and attempted to transfer to a different sphere at an altitude of 61.5 km, descending. After a several-minute search, the first sphere was finally reacquired and tracked until it deflated at the normal altitude.

When the system design was initiated, sphere deployment and inflation

problems were anticipated. We believe that an adequate degree of reliability was finally achieved. Except for the first two soundings, all spheres tracked to a low altitude deflated at the expected level. The trajectory of the first rocket was abnormal due to marginal stability. Only the first sphere was observed to eject, and inflation was not successful. The initial explanation of the difficulty was ejection at low altitude where drag and heating were more severe. Later, we found that the sphere of sounding 8 survived a similar ejection. The trajectory and ejection problems of the first sounding were corrected for the second. This time, after a successful inflation, the sphere deflated prematurely. A possible explanation for the deflation of this sphere was failure of the isopentane capsule to release inflation gas. The inflation that was seen may have been due to a small amount of air trapped in the sphere when it was packed. The pneumatically operated capsule used for the first two soundings was therefore abandoned, and an inertia-operated capsule was developed for use on all subsequent soundings (Figure 5). The new capsule enabled us to vent the space in which the sphere was packed so that any air outside the sphere could escape prior to ejection. This change may have been an important factor in the more successful later soundings. When the results of all soundings were compared, we found that the second sounding indicated above-average atmospheric density. This may have been caused by a loss of isopentane through a damaged sphere envelope. The derived density was relatively high in one other case, that of the ascending profile of sounding 12. In this case it is not known where the ascending sphere deflated because a different sphere was tracked on descent.

The Tradex is capable of recording all the target signal returns within the radar beam. The Precision Radar Recorder preserves ungated, undetected radar signals at IF along with other reference signals. The device has limited usefulness in the falling-sphere system, since on a typical shot all three spheres remain in the 2° radar beam only on ascent and on a small portion of descent. The recording time is limited to approximately 5 minutes, but the spheres require 18 minutes to descend to 30 km altitude. The IF recorder was a useful back-up on the third firing when the primary data-recording system failed to record until the sphere had descended to an altitude of 47 km. All the high-altitude results of this firing were recovered from the IF recording.

The antenna motion of the Tradex radar is limited in azimuth in that a dead-zone sector cannot be entered. This problem was encountered on the fourth firing when the sphere trajectory entered the dead zone. The action taken then was to plunge the antenna, that is to break track on the sphere, slew the antenna 180° in azimuth and increase the elevation angle beyond 90°, and reacquire the sphere. Although the procedure was successful in reacquiring the sphere near apogee, the bulk of the ascending tracking data was lost in this shot.

Digital data were recorded on magnetic tape by the Tradex radar. Range, range rate, azimuth, and elevation were each sampled at a rate of 10 per second. Analog as well as digital recordings of target cross section were also supplied. The radar facility included an IBM 7090 data processor which enabled us to deliver atmospheric profiles the day of the sounding. The raw-

insonde temperature profiles were measured by a precision thermistor. Three different techniques were used for pressure: Pressure profiles were measured by an aneroid cell, or hypsometer, or were derived from altitude data measured by the GMD-2 instrument. We believe that equal accuracy can be obtained with either the hypsometer or the GMD-2, and less accuracy with the aneroid cell.

## DATA ANALYSIS PROCEDURES

An orthogonal system of coordinates is used based on the radar coordinates range, azimuth, and elevation angle (Figure 7). In this system of spherical coordinates, the velocity components are:

$$\begin{aligned} V_1 &= \dot{r} \\ V_2 &= r\dot{\epsilon} \\ V_3 &= r \cos\epsilon \, \dot{\alpha} \end{aligned} \tag{1}$$

where $\dot{r}$ is the range rate, and $\dot{\alpha}$ and $\dot{\epsilon}$ are the azimuth and elevation-angle rates in radians per second. The acceleration components are:

$$\begin{aligned} a_1 &= \ddot{r} - (V_2^2 + V_3^2)/r + a_{cor\ 1} + a_{cen\ 1} \\ a_2 &= r\ddot{\epsilon} + 2\, V_1 V_2/r + V_3^2 \tan\epsilon/r + a_{cor\ 2} + a_{cen\ 2} \\ a_3 &= r\ddot{\alpha} \cos\epsilon + 2\, V_1 V_3/r - 2\, V_2 V_3 \tan\epsilon/r + a_{cor\ 3} + a_{cen\ 3} \end{aligned} \tag{2}$$

The Coriolis and centrifugal accelerations are present because the radar coordinates are not an inertial system but rotate with the earth. These accelerations have a small effect, except at the highest altitudes, but are in-

cluded in the calculations. The Coriolis and centrifugal accelerations are most conveniently written as vector cross products:

$$\begin{aligned} \vec{a}_{cen} &= \vec{\Omega} \times (\vec{\Omega} \times \vec{R}) \\ \vec{a}_{cor} &= 2\,\vec{\Omega} \times \vec{V} \end{aligned} \tag{3}$$

where $\vec{V}$ is defined by (1) and where the components of the earth rotation rate are:

$$\begin{aligned} \Omega_1 &= \Omega(\sin L \sin\epsilon + \cos L \cos\alpha \cos\epsilon) \\ \Omega_2 &= \Omega(\sin L \cos\epsilon - \cos L \cos\alpha \sin\epsilon) \\ \Omega_3 &= -\Omega \cos L \sin\alpha \end{aligned} \tag{4}$$

and the components of the geocentric radius are:

$$\begin{aligned} R_1 &= r_e \sin\epsilon + r \\ R_2 &= r_e \cos\epsilon \\ R_3 &= 0 \end{aligned} \tag{5}$$

The constants for earth rotation rate, earth equatorial radius, and the latitude of Roi-Namur Island are:

$$\begin{aligned} \Omega &= 7.292 \times 10^{-5} \text{ rad/sec} \\ r_e &= 6{,}378{,}388 \text{ meters} \\ L &= 9°24' \text{ North} \end{aligned} \tag{6}$$

An adequate approximation is to use a constant latitude when computing the small centrifugal accelerations. The components of gravity needed for the

data analysis are:

$$\begin{aligned} g_1 &= -g \cos\beta \\ g_2 &= -g \sin\beta \\ g_3 &= 0 \end{aligned} \tag{7}$$

where the gravity at altitude is related to gravity at sea level by the inverse-square law.

$$g = g_s \, r_e^2/R^2 \tag{8}$$

The geocentric radius R and the angle $\beta$ between the range vector and the vertical can be found by solving the geocentric triangle (Figure 8).

$$\begin{aligned} R &= \sqrt{r_e^2 + 2\, r_e r \sin\epsilon + r^2} \\ \cos\beta &= (r_e \sin\epsilon + r)/R \\ \sin\beta &= r_e \cos\epsilon/R \end{aligned} \tag{9}$$

Gravity at sea level is computed from the formula:

$$g_s = 978.049(1 + 0.0052884 \sin^2 L - 0.0000059 \sin^2 2L) + r_e \, \Omega^2 \cos^2 L \tag{10}$$

which is the international gravity formula [Wolfe, 1958] with a centrifugal acceleration term added.

The equations of motion are derived by assuming that there are no lateral forces (lift). The drag force, by definition, is directed opposite to the motion of the sphere relative to the air mass. The equations of motion are three in number, corresponding to the three degrees of freedom of a falling

sphere. However, four atmospheric parameters influence the motion of the sphere, namely air density and the three wind components. The indeterminate system of equations can be solved by assuming the vertical wind component to be zero. This particular choice is dictated by both meteorological and system considerations. Vertical wind motion is believed to be relatively small. Second, the sphere trajectory is approximately vertical. It is obvious that the component of wind tangent to the trajectory cannot be distinguished from a change of air density since both influence the same component of drag; drag is, of course, the measured quantity.

The form of the equation of motion used depends on the portion of the trajectory being considered. On the ascending part of its trajectory, the sphere is at a high altitude and has a large velocity, about 1000 m/sec. Lateral winds have a relatively small influence on the trajectory due to the large sphere velocity and small air density. A single component of the equations of motion was therefore used, suppressing the wind calculation. The equation of motion associated with the range vector direction provides the air density equation,

$$ma_1 = \frac{1}{2} C_D A \rho V V_1 \tag{11}$$

where

$$V = \sqrt{V_1^2 + V_2^2 + V_3^2} \tag{12}$$

and m, $C_D$, and A are the mass, drag coefficient, and cross section area of the sphere. Equation (11) may be solved for the density. The acceleration $a_1$ can

be developed according to equations (2) and (3) to obtain (13)

$$\rho = \frac{2m}{C_D A V V_1}\left\{g_1 - \ddot{r} + (V_2^2 + V_3^2)/r - \left[\vec{\Omega}x(\vec{\Omega}x\vec{R})\right]_1 - 2(\vec{\Omega}x\vec{V})_1\right\} \quad (13)$$

The only large acceleration terms in equation (13) are $g_1$ and $\ddot{r}$. However, the difference between these two is small, about one per cent of g at 120 km. The other terms, though small, are therefore significant. Favorable characteristics of equation (13) are that the second derivatives of azimuth and elevation angle are not involved, and the azimuth and elevation velocity components are relatively small. The accuracy of the system is therefore limited by the accuracy of range acceleration. Since the Tradex radar delivers range-rate data, only a single differentiation is required to obtain range acceleration. These factors result in very sensitive measurements of drag at high altitude.

On the descending portion of the sphere's trajectory, below 70 km, the horizontal components of wind are included in the calculations, and all three equations of motion are used. In vector form the equation of motion is:

$$m(\vec{a} - \vec{g} - \vec{a}_b) = -\frac{1}{2} C_D A \rho v \vec{v} \quad (14)$$

The velocity v relative to the air mass is:

$$v = \sqrt{(V_x - W_x)^2 + (V_y - W_y)^2 + V_z^2} \quad (15)$$

$\vec{a}_b$ is the upward acceleration due to buoyancy,

$$\vec{a}_b = \frac{\pi d^3}{6m} \rho \vec{g} \tag{16}$$

where d is the sphere diameter. Writing equation (14) in component form gives

$$\begin{aligned} \rho &= -2m(a_z + g - a_b)/C_D A v V_z \\ W_x &= V_x + 2ma_x/C_D A \rho v \\ W_y &= V_y + 2ma_y/C\ A\rho v \\ W_z &= 0 \end{aligned} \tag{17}$$

The coordinates x, y, and z are associated with the downrange, crossrange, and vertical directions. Equations (17) can be put into a better form for computational purposes by eliminating density from the wind equations to give,

$$\begin{aligned} \rho &= -2m(a_z + g - a_b)/C_D A v V_z \\ W_x &= V_x - a_x V_z/(a_z + g - a_b) \\ W_y &= V_y - a_y V_z/(a_z + g - a_b) \\ W_z &= 0 \end{aligned} \tag{18}$$

The components of velocity and acceleration which appear in (18) are related to the radar-coordinate components (1) and (2) by the following equations:

$$\begin{aligned} V_x &= V_1 \sin\beta - V_2 \cos\beta \\ V_y &= V_3 \\ V_z &= V_1 \cos\beta + V_2 \sin\beta \end{aligned} \tag{19}$$

$$
\begin{aligned}
a_x &= a_1 \sin\beta - a_2 \cos\beta \\
a_y &= a_3 \\
a_z &= a_1 \cos\beta + a_2 \sin\beta
\end{aligned}
\tag{20}
$$

Equations (18) are not an explicit solution for the density $\rho$ because the drag coefficient $C_D$ depends on both the density and the temperature according to an involved empirical formula. The buoyancy acceleration $a_b$ also depends on the density. The equation was therefore solved by an iteration process. Equations (18) are almost an explicit solution for the wind components $W_x$ and $W_y$ because, except for the buoyancy acceleration, all terms can be derived directly from the radar data. It was not necessary to iterate the wind components because improvements were negligible.

Above 70 km the horizontal wind components have a relatively small influence on the sphere trajectory due to the large sphere velocity and small air density. Between 65 and 70 km, the wind profiles derived were more scattered, indicating the presence of a sensitivity threshold. Therefore, above 70 km the wind calculation was suppressed, and the equations of motion (18) reduced to:

$$\rho = -2m(a_z + g - a_b)/C_D A V V_z \tag{21}$$

where

$$V = \sqrt{V_1^2 + V_2^2 + V_3^2} \tag{22}$$

Equation (21), applicable to the descending sphere trajectory, is similar to

equation (13), applicable to the ascending sphere trajectory, except that vertical components rather than range components are used.

One must retrieve from the radar data the rates and accelerations required by the equations of motion. This can be accomplished by fitting a second-degree polynomial to a number of data points using a least-squares formula. If 2m + 1 data points are used, equally spaced in time and symmetrical about $t_o$, at a rate f per second, then the required second-degree polynomial is:

$$x = x_o + \dot{x}_o(t-t_o) + \frac{1}{2}\ddot{x}_o(t-t_o)^2 \tag{23}$$

where $-m/f \leq t - t_o \leq m/f$. The formulas for the coefficients are:

$$x_o = \frac{3}{4(2m+1)\left[(2m+1)^2 - 4\right]} \sum_{k=-m}^{k=+m} \left[3(2m+1)^2 - 7 - 20k^2\right] x_k \tag{24}$$

$$\dot{x}_o = \frac{3f}{m(m+1)(2m+1)} \sum_{k=-m}^{k=m} k\, x_k \tag{25}$$

$$\ddot{x}_o = \frac{30f^2}{(4m^2-1)(2m+3)} \sum_{k=-m}^{k=+m} \left(\frac{3k^2}{m(m+1)} - 1\right) x_k \tag{26}$$

The rate f was always 10 data points per second. Formulas (24), (25), and (26) were derived specifically for this application. Similar formulas are given by Worthing and Geffner [1943]. Equation (26) was used to derive the second derivative of the azimuth and elevation angles. Equation (25) was

used to derive angle rates. Equation (25), operating on range-rate data, was also used to derive the second derivative of the range. Equation (24) is included for completeness but was not needed because the raw data were sufficiently accurate. On the ascending sphere trajectory, a single quadratic function was fitted to all the applicable elevation-angle data, about 40 seconds of tracking, and was used to derive the angle rate. The azimuth data were treated in the same way. The root-mean-square differences between these functions and the raw angle data were calculated for each firing and were used as indicators of radar performance. A variable number of data points were used to derive $\ddot{r}$ depending on the accuracy required, which is a function of altitude. At 120 km, all data points in a 10-km altitude band were used. Figure 9 shows the complete function. Different ways of processing the ascending sphere data were tried, all of which indicated that the range-rate information was the controlling factor and that practically any treatment of the angle information gave satisfactory results. On the descending portion of the sphere trajectory, errors in the angle data have a larger effect due to geometrical factors. The altitude band used to derive angle rates and accelerations ranged from 3 to 10 km and was double the bandwidth used to derive range acceleration from the relatively accurate range-rate data (Figure 9).

Falling spheres measure atmospheric density directly. It is desired to derive pressure and temperature profiles as well. This can be done by using the hydrostatic and state equations:

$$\frac{dP}{dz} = -\rho g$$
$$P = \rho RT \qquad (27)$$

These equations may be solved for the molecular scale temperature

$$T = \frac{-1}{R\rho} \int \rho g dz \qquad (28)$$

The temperature equation has two properties of particular interest in this application. Density appears in both numerator and denominator. Errors that have their source in the drag coefficient or the density therefore tend to cancel. If density errors were monotonic, for example, equation (28) requires the per cent temperature error to be smaller than the per cent density error. If all drag coefficients were in error by a constant factor, the correct temperature profile would be derived through the use of wrong drag coefficients. In a practical case, the drag-coefficient error is unknown and variable, but the temperature-profile error is probably smaller than the density-profile error. A second point of interest is that the hydrostatic equation is differential. A pressure profile derived by integration is therefore offset by an indeterminate constant. A similar offset occurs in the derived temperature profile. The procedure adopted was to use the standard atmosphere temperature at the highest altitude on the temperature profile. The pressure offset can then be determined and the complete pressure and temperature profiles derived. Errors introduced by this procedure can be studied by assuming an isothermal atmosphere. One can show, in this case, that when the altitude is decreased one scale height the temperature error and the per cent pressure error each are decreased by the factor e = 2.718.

The highest point of the profile is determined by the quality of the data found in each particular case. Beginning at very high atltitude, eleven values of $C_D\rho$ are found which span 10 km. A least-squares straight line is fitted to the logarithms of the eleven values of $C_D\rho$. If any $C_D\rho$ falls more than 20 per cent from the straight line, the data are rejected as not good enough and the process is repeated at an altitude 1 km lower. The starting point is therefore appropriate for each set of data and may be different for different firings. This is done on both ascending and descending profiles. At 120 km, the acceleration due to drag is approximately 10 cm/sec$^2$ (one per cent of g). Simulation studies using estimated radar errors indicated that good results could not be expected at higher altitudes, therefore all profiles were terminated at 120 km.

## DRAG COEFFICIENTS

As the sphere falls from its highest altitude where drag is measurable, about 120 km, to the altitude of sphere deflation, about 30 km, a wide range of aerodynamic parameters is covered. At the highest altitude, where Knudsen number is large, the theoretical free-molecule flow equation for diffuse reflection is used [Schaaf and Chambre, 1961]:

$$C_{D_{FM}} = \frac{1 + 2S^2}{\sqrt{\pi}\, S^3} e^{-S^2} + \left(2 + \frac{2}{S^2} - \frac{1}{2S^4}\right) \mathrm{erf}(S) + \frac{2\sqrt{\pi}}{3S_w} \qquad (29)$$

The speed ratio S is the ratio of sphere velocity to the most probable molecular velocity,

$$S = V/\sqrt{2RT}$$

The temperature T is computed from the derived density profiles by an iterative process. The speed ratio $S_W$ depends on the temperature of the sphere. It is assumed that there is no significant transfer of heat to the sphere surface during its brief flight, so that $T_W = 300°K$. Speed ratio and Mach number are related by the formula

$$S = \sqrt{\gamma/2}\, M$$

where $\gamma = 1.4$. The variability of molecular weight with altitude is not included in this analysis. Molecular scale temperature is derived therefore rather than kinetic temperature. Below 108 kilometers, approximately, the Knudsen number becomes smaller than unity, and the sphere drag measurements of Ashkenas [1962], Wegener and Ashkenas [1961], Aroesty [1962], and Sreekanth [1962] become applicable. These measurements indicate that the variability of drag coefficient with Mach number is not large for Mach numbers in the range 2 to 4. A drag-coefficient function of Reynolds number, independent of Mach number, is therefore used. Table 4 shows the values of $C_{D_R}$ used, based mainly on the measurements by Ashkenas [1962]. Near Knudsen number of 1, use of either the free-molecular formula or the wind-tunnel measurements requires an extrapolation. In this range, the drag coefficient is found by the formula

$$\frac{C_D - C_{D_R}}{C_{D_{FM}} - C_{D_R}} = 1 \qquad \text{for} \qquad K > 10$$

$$= \frac{1}{2} + \frac{3}{4} u - \frac{1}{4} u^3 \qquad 0.1 < K < 10 \qquad (30)$$

$$= 0 \qquad K < 0.1$$

where $u = \log_{10} K$. When $K = 1$, the formula reduces to

$$C_D = \frac{1}{2}\left(C_{D_R} + C_{D_{FM}}\right)$$

Knudsen number, Mach number, and Reynolds number are related by the formula

$$K = 1.26 \sqrt{\gamma}\, M/Re \qquad (31)$$

These coefficients are in agreement with those derived by Sherman, who analyzed a similar falling-sphere problem [Faucher et al., 1963]. Equation (30) was designed to agree with Sherman, although the form is different because in this case it was necessary to find an equation applicable to low as well as to high altitudes. As the sphere falls into the dense air at low altitude, the drag increases until the sphere velocity becomes subsonic. Drag coefficients have been measured by Heinrich for Mach numbers less than 0.9 at the necessary Reynolds numbers [Engler, 1962]. The supersonic and subsonic drag-coefficient functions from the above sources are relatively accurate. At transonic Mach numbers the drag coefficient abruptly changes by a factor of 2 approximately. Unfortunately, data for this area are more scanty. The measurements by May [1957] are used here. The Mach number falls from 2.0 to 1.0 between 78 and 72 km, approximately. Transonic Mach numbers always occur at

a specific altitude, which is a function of sphere mass-to-area ratio and air density. Table 5 shows the drag coefficients used at low altitude when Mach number is less than 2.5.

## INTERPRETATION OF THE ATMOSPHERIC PROFILES

Useful results were obtained from thirteen of the sixteen soundings (Figures 10 - 22). The time of rocket firings and rawinsonde releases are given for Greenwich Mean Time; local time at Kwajalein is 12 hours different from GMT.

Since density and molecular scale temperature profiles were obtained on both ascent and descent, a comparison of the two provided a check on the consistency of results. In several cases the agreement was very satisfactory. In general, when differences between the two density profiles occur, the ascending profile should be given greater weight. Two factors are present: 1) The ascending trajectory enjoys more favorable geometry, which minimizes the effects of inaccurate radar azimuth and elevation angles. 2) The overlapping portion is small, and the connection occurs at the lower end of the ascending profile where it is most accurate, and at the upper end of the descending profile where it is least accurate. An exception may occur when it is impossible to verify the mass of the ascending sphere. In the case of soundings 7, 8, 13, 14, 15, and 16, the ascending sphere was also tracked on descent and was observed to deflate near 30 km altitude, approximately 18 minutes after deployment. It can be assumed that the mass of isopentane es-

caping from these spheres was insignificant. In the case of soundings 2, 3, 4, and 12, different spheres were tracked ascending and descending (cf. Table 1). Consequently an absolute check of the integrity of the ascending sphere was impossible. The loss of 8 grams of isopentane from a sphere of gross weight 50 grams would result in a spurious calculated density equal to 50/42 of the correct density. The sphere might be expected to lose its shape due to the loss of internal pressure. The radar AGC record of each ascending sphere was carefully examined for an indication of change of shape, but no indication was found. The low atmospheric pressure and the low drag at high altitude may not be sufficient to cause an observable collapse.

The ascending profile (first sphere) and the descending profile (third sphere) of sounding 2 indicate above average density (Figure 10). The third sphere was observed to deflate prematurely. The second sphere was tracked for 10 seconds at very high altitude and appeared to accelerate abnormally in a way that might have been caused by the reaction of a jet of escaping gas. Abnormalities in the profiles of the other three soundings of this group, 3, 4, and 12, are not suspected for any specific reason, although in the case of 12 the agreement between the two profiles is not as satisfactory as in others.

In the case of temperature profiles, an additional factor must be considered: The initial temperature at the highest altitude of a profile was always made equal to the standard atmosphere temperature, which was not necessarily an accurate measure of the correct temperature. Any error diminishes at an exponential rate at lower levels, but may be important at the upper end of the descending profile where comparisons are made with the ascending profile.

Near 30 km the rawinsonde measurements also provided a valuable check. In most cases the agreement between sphere and rawinsonde was satisfactory. It may be significant that the poorest agreement was found in those cases in which rawinsonde releases were not well coordinated with the rocket launch. The sphere profiles were terminated near 30 km when the sphere collapsed because of increased ambient pressure. The drag of a sphere in an advanced state of collapse is known to be greater than that of a fully inflated sphere. Deflation would therefore cause a spurious increase in derived air density and a corresponding decrease in derived temperature. The collapse of a sphere can always be seen in the radar AGC data, possibly when deflation has reached an advanced state. Since the altitude pressure gradient is quite large, the sphere cannot be in a state of partial deflation through a great altitude range. All the sphere profiles were terminated above the altitude where radar AGC first indicated deflation. The rawinsonde data always followed the tropical 15° N model atmosphere quite closely. The profile of density ratio departs significantly from unity near 16 km because the reference density used was the U. S. Standard, 1962. The tropical 15° N model atmosphere would have been more applicable near the tropopause but is not defined at high altitude.

The interpretation of the density and temperature profiles near 70 km requires special care. In a typical trajectory, the sphere passes through the transonic range of Mach numbers between 69 and 73 km (Table 3). In this range, the sphere drag coefficient is known with less accuracy than at other altitudes. Perhaps of equal importance is the variability of the

drag. As the sphere passes through the transonic range, the drag coefficient decreases approximately 50 per cent. The great variability of the drag is undoubtedly a source of error when retrieving rates and accelerations from the raw radar data. Since the density profiles consistently indicate a density increase when the sphere is falling at or near the 70 km level, one must suspect that these two difficulties are contributing factors. This characteristic of the density-ratio profile is, of course, also reflected in the temperature profile. The altitude at which sphere Mach number is equal to 1 is shown on each density profile (Figures 10 - 25) and also the altitude at which sphere Knudsen number is 1, approximately 108 km.

An inspection of the different profiles reveals a number of interesting features.

1) Near 50 km the derived temperature is always 10 to 30 degrees higher than the U. S. Standard, 1962. In this area, the drag coefficients are believed to be relatively good. An error of 2 per cent or less is claimed for the drag coefficient measurements made by Heinrich [Engler, 1962]. Any temperature error associated with transonic drag problems at 70 km would have decayed to a small value at the 50-km level.

2) The measurements tend to confirm the general characteristics of mesopause structure defined by the U. S. Standard, 1962 model atmosphere, but indicate a somewhat lower temperature than 180°K and places the mesopause at a somewhat higher level than 80 to 90 km. The presence of diurnal or seasonal variations is also indicated, but these are more difficult to define with the limited number of soundings at hand. At the 90 to 100-km levels it

can be argued that the system lacks accuracy because only descending data are applicable. It must be admitted that any individual profile might be discounted for this reason. In this case, however, many profiles indicate a similar effect, and at 100 km the more accurate ascending data tend to confirm the descending profiles. The lowest mesopause temperature, 126°K at 94 km, was measured by sounding 4, 0300 GMT, 20 June 1963. Only a small amount of ascending data was obtained on this sounding; this data also indicated a temperature lower than the standard.

3) The six soundings of May and June all exhibit a local temperature maximum near 85 km. The phenomenon is absent in four soundings in the months of January, March, and November, but can be seen in the sounding of 13 March 1964. These temperature profiles suggest the presence of heating effects smmilar to those in the polar winter mesosphere measured with falling spheres by Jones et al. [1959], and discussed by Kellogg [1961] and Young and Epstein [1962]. At the present time there is no theory for warmings of the tropical mesosphere. A similar but smaller effect can be seen near the 72-km level. At 72 km the measurements do not decisively indicate an atmospheric phenomenon since this is also the area of transonic sphere drag-coefficient problems.

4) The lowest point of the ascending profiles usually falls near the 100-km level. Of ten soundings, nine indicated a lower temperature than the standard at the base of the profile. A variety of patterns can be seen in the ascending profiles, some of which suggest heating effects. Simulation studies were undertaken to determine if radar errors were an important factor. The results were inconclusive. We found that during sphere ascent, the

azimuth, the elevation, and the range were not important sources of error. The range-rate data were believed to be accurate to within less than one meter per second. When cyclical range-rate errors were assumed, it was possible to simulate the variations seen in the ascending density and temperature profiles. It may be more realistic to assume constant error, or error dependent on velocity or on acceleration. Such errors would probably have a smaller effect than the observed variations. All ascending profiles were arbitrarily terminated at 120 km, although the limit based on smoothness would have had effect at a higher altitude. The smoothness criterion used on the descending profiles required scatter less than 20 per cent when eleven values of $C_D\rho$, which spanned 10 km, were examined. At 120 km the sphere acceleration due to drag was approximately 10 $cm/sec^2$.

5) Figure 23 shows the results of the day-night pair of soundings of 18 June 1964. The first sounding was at 2:19 P.M., local time, and the second sounding was approximately fourteen hours later, at 4:30 A.M. The second sounding was just prior to sunrise, with the atmosphere in darkness at the highest altitude of measurement. The two temperature profiles agree very closely from 32 km to 96 km, except for the band from 78 to 81 km, where there is an indication of heating in the night profile. The generally close agreement would seen to indicate that the accuracy and repeatability of falling-sphere measurements are very good. However, the corresponding density profiles, which are the more fundamental measurements, indicate daytime density approximately 10 per cent greater than nighttime density. In this case, the rawinsonde data do not confirm the night sphere data. Unfortunately, the re-

lease of the rawinsonde was not well coordinated with the rocket launch and can be discounted for this reason. The possibility of an erroneous sphere mass or diameter was excluded after a critical review of all procecures. One can speculate that the difference in the density profiles might be explained by tides in the atmosphere [Siebert, 1961]. A tidal or gravity wave of thermal and/or gratitational origin, having the effect of lowering the air mass less than 1 km between the day and the night firing, would be sufficient to cause the observed difference between the density profiles and the lack of change in the temperature profiles.

6) The average and extreme density and temperature results are plotted in Figure 24 for the five soundings in June, and in Figure 25 for all thirteen soundings, including June. The envelope profiles associated with the descending trajectories were terminated at 90 km. At higher altitudes the descending profiles become less reliable, and since the envelope would be formed by the most severely scattered profiles of the group, it was thought that questionable inferences might be drawn from the deleted data. No great differences can be seen between Figures 24 and 25 and the day-night pair, Figure 23. This result indicates that at this latitude seasonal changes may be relatively small compared to diurnal changes.

## CONCLUSIONS

This series of soundings demonstrated that the falling-sphere system is well suited to certain measurement problems in the atmosphere as high as

mesopause or lower thermosphere. The system appears to be capable of resolving atmospheric changes which span a small altitude range, of the order of 1.0 km. The payload is relatively economical, so that measurements on a larger scale may be feasible. The phenomena of warmings near mesopause and large diurnal variations in the density profile indicate that more soundings at tropical and other latitudes are desirable.

## ACKNOWLEDGMENTS

We wish to acknowledge the financial support of the Pacific Missile Range for this specific task and the cooperation of J. E. Masterson.

The development of falling sphere systems is a continuing program at this laboratory supported by the National Aeronautics and Space Administration. Our work with radar tracked spheres was first encouraged by M. Dubin.

In addition to the authors a number of workers made valuable contributions. At the High Altutide Engineering Laboratory we wish to mention specifically L. M. Jones and H. F. Allen. Dr. Allen's work with sphere development was at times as intensive as our own. P. B. Hays and C. Young contributed to our interpretation of the atmospheric profiles. J. R. Sandlin, RCA, Kwajalein was most helpful with interpretation of radar data and data processing. H. E. Boyd, Meteorologist in charge, PMR Weather Station, Kwajalein conducted rawinsonde measurements and experimental sphere releases. A. Gephard, Viron Division, GCA, directed sphere fabrication and packaging. S. P. Bean, New Mexico State University, supervised rocket launch operations at Kwajalein.

# REFERENCES

Aroesty, J., Sphere drag in a low density supersonic flow, Univ. Calif. Tech. Rept., HE-150-192, Berkeley, 1962.

Ashkenas, H. I., Sphere drag at low Reynolds numbers and supersonic speeds, Jet Propulsion Laboratory Research Summary, No. 36-12, Vol. 1, 1962.

Bartman, F. L., L. W. Chaney, L. M. Jones, and V. C. Liu, Upper air density and temperature by the falling sphere method. J. Appl. Phys., 27, 706-712, 1956.

Committee on Extension to the Standard Atmosphere, U. S. Standard Atmosphere, 1962, Superintendent of Documents, U. S. Government Printing Office, Washington, D.C.

Engler, N. A., Development of methods to determine winds, density, pressure, and temperature from the ROBIN falling balloon, A. F. Cambridge Research Laboratories, Bedford, Mass., 1962.

Faucher, G. A., R. W. Procunier, and F. S. Sherman, Upper atmosphere density obtained from measurements of drag on a falling sphere, J. Geophys. Res., 68, 3437-3450, 1963.

Jones, L. M., J. W. Peterson, E. J. Schaefer, and H. F. Schulte, Jr., Upper air density and temperature: some variations and an abrupt warming in the mesosphere, J. Geophys. Res., 64, 2331-2340, 1959.

REFERENCES (Continued)

Kellogg, W. W., Warming of the polar mesosphere and lower ionosphere in the winter, J. Meteorol., 18, 373-381, 1961.

Lenhard, R. W., Variation of hourly winds at 36 to 65 kilometers during one day at Eglin Air Force Base, Florida, J. Geophys. Res., 68, 227-234, 1963.

Leviton, R., and J. B. Wright, Accuracy of density from the ROBIN falling sphere, GRD Res. Notes No. 73, Geophysics Research Directorate, A. F. Cambridge Research Laboratories, Bedford, Mass., 1961.

May, A., Supersonic drag of spheres at low Reynolds numbers in free flight, J. Applied Physics 28, 910-912, 1957.

Peterson, J. W., and K. D. McWatters, The measurement of upper air density and temperature by two radar-tracked falling spheres, NASA Contractor Report CR-29, April 1964.

Schaaf, S. A., and P. L. Chambre, Flow of Rarefied Gases, Princeton Aeronautical Paperbacks, Princeton University Press, 1961.

Siebert, M., Atmospheric tides, in Advances in Geophysics, Vol. 7, edited by H. E. Lansberg and J. Van Mieghem, pp. 105-187, Academic Press, New York, 1961.

REFERENCES (Concluded)

Sreekanth, A. K., Drag measurement on circular cylinders and spheres in a highly rarefied gas stream at a Mach number of two, ARS J., 32, 748-754, 1962.

Wegener, P. P., and H. I. Ashkenas, Wind tunnel measurements of sphere drag at supersonic speeds and low Reynolds numbers, J. Fluid Mech., 10, 550-560, 1961.

Wolfe, H. C., Gravitation, in Handbook of Physics, edited by E. U. Condon and H. Odishaw, Part 2, pp. 55-59, McGraw-Hill Book Company, New York, 1958.

Worthing, A. G., and J. Geffner, Treatment of Experimental Data, pp. 238-269, John Wiley and Sons, Inc., New York, 1943.

Young, C., and E. S. Epstein, Atomic oxygen in the polar winter mesosphere, J. Atmospheric Sci., 19, 435-443, 1962.

# LIST OF TABLES

TABLE 1 Summary of Kwajalein Sphere Firings

TABLE 2 Computer Output, Typical Firing, Ascending Data

TABLE 3 Computer Output, Typical Firing, Descending Data

TABLE 4 Drag Coefficient Used When Mach Number Exceeds 2.5

TABLE 5 Drag Coefficient Used when Mach Number Is Less Than 2.5

TABLE 1. Summary of Kwajalein Sphere Firings*

| Sounding Number | Time and Date GMT | p, ρ, T Profiles km | Sphere Tracked | Ejection Altitude km | Time of Lock-on Sphere 1 sec | Sphere 1 Velocity at 120 km m/sec | Sphere Apogee km | RMS Error Az mils | RMS Error El mils | Remarks |
|---|---|---|---|---|---|---|---|---|---|---|
| 1 | 0130 26 March 1963 | - | 1 | 77.4 | 96.5 | - | 93 | -- | -- | Abnormal trajectory. Ejection at 67 sec. No inflation. |
| 2 | 0257 29 March 1963 | 100 - 120<br>102 - 65 | 1<br>3 | 90.7 | 79.0 | 716 | 146<br>177 | 1.62 | 0.16 | Ejection at 72 sec. Premature deflation at 62.2 km, descending |
| 3 | 0328 18 June 1963 | 99 - 120<br>102 - 73<br>44 - 33 | 1<br>2<br>2 | 86.5 | 95.5 | 788 | 151<br>177 | 0.88 | 0.18 | Radar-data recording incomplete. Playback data used. |
| 4 | 0300 20 June 1963 | 104 - 110<br>98 - 33 | 1<br>3 | 86.0 | 85.0 | - | 150<br>180 | -- | 0.33 | Incomplete radar track, ascending. |
| 5 | 1031 4 Nov. 1963 | 45 - 40 | ? | -- | -- | - | - | -- | -- | Incomplete radar track. |
| 6 | 1226 4 Nov. 1963 | 45 - 32 | ? | -- | -- | - | - | -- | -- | Incomplete radar track. |
| 7 | 1626 9 Nov. 1963 | 107 - 120<br>103 - 37 | 1<br>1 | 83.7 | 91.0 | 648 | 141 | 1.28 | 0.14 | Results essentially complete.<br>Data-recording problem at 34.4 km, descending |
| 8 | 1458 14 Nov. 1963 | 104 - 120<br>109 - 64<br>38 - 32 | 1<br>1<br>1 | 77.9 | 95.0 | 390 | 127 | 2.23 | 0.27 | Premature break track at 61.5 km, descending. |
| 9 | -- 18 Dec. 1963 | - | - | -- | -- | - | - | -- | -- | No radar track. |
| 10 | -- 18 Dec. 1963 | - | - | -- | -- | - | - | -- | -- | No radar track. |
| 11 | 1825 23 Jan. 1964 | 98 - 33 | 1 | -- | 123.6 | - | 172 | -- | -- | No radar track ascending. |
| 12 | 1820 13 March 1964 | 99 - 120<br>104 - 32 | 1<br>2 | 82.0 | 82.0 | 575 | 136<br>174 | 0.71 | 0.10 | Results complete. |
| 13 | 1125 12 May 1964 | 96 - 120<br>107 - 37 | 1<br>1 | 83.9 | 79.0 | 690 | 144 | 1.38 | 0.11 | Results essentially complete.<br>Data-recording problem at 35.1 km, descending. |
| 14 | 0101 17 June 1964 | 102 - 120<br>102 - 32 | 1<br>1 | 84.4 | 85.0 | 626 | 140 | 3.33 | 1.58 | Results complete. |
| 15 | 0219 18 June 1964 | 100 - 120<br>98 - 32 | 1<br>1 | 85.5 | 81.1 | 753 | 149 | 1.23 | 0.60 | Results complete. |
| 16 | 1630 18 June 1964 | 102 - 120<br>100 - 32 | 1<br>1 | 85.6 | 83.0 | 745 | 148 | 1.88 | 1.13 | Results complete. |

*When pressure, density, and temperature profiles resulted for both descending and ascending sphere trajectories, the ascending profile is listed first followed by the descending profile or profiles.

The ejection altitude of the first sphere is the rocket altitude at the expected time of ejection, which was 70 seconds after lift-off for all shots except the first two.

When different spheres were tracked ascending and descending, the apogee altitude of the ascending sphere is listed first followed by the apogee altitude of the descending sphere.

The root-mean-square error of azimuth and elevation angles is computed on the ascending part of the trajectory using approximately 40 seconds of data but is probably applicable to the entire flight. One mil = 0.05625°.

TABLE 2. Computer Output, Typical Firing, Ascending Data

| ALTITUDE KM | DENSITY KG/CU.M | TEMP K | PRESSURE MILLIBAR | CD | RE | MACH | KNUDSEN | SPEEDR | TOTVEL M/S | DELZ KM | XDB VAR |
|---|---|---|---|---|---|---|---|---|---|---|---|
| 120.01 | 1.42 -8 | 361 | 1.47 -5 | 3.704 | 2.78-1 | 1.64 | 8.81 | 1.38 | 626.3 | 10.0 | |
| 119.00 | 1.57 -8 | 358 | 1.61 -5 | 3.637 | 3.17-1 | 1.69 | 7.94 | 1.41 | 641.1 | 9.4 | .49 |
| 118.00 | 1.90 -8 | 327 | 1.78 -5 | 3.501 | 4.19-1 | 1.81 | 6.43 | 1.51 | 655.9 | 8.9 | .52 |
| 117.03 | 2.40 -8 | 287 | 1.97 -5 | 3.341 | 5.99-1 | 1.97 | 4.91 | 1.65 | 669.9 | 8.4 | .53 |
| 116.01 | 3.05 -8 | 256 | 2.23 -5 | 3.198 | 8.50-1 | 2.13 | 3.74 | 1.79 | 684.7 | 7.9 | .45 |
| 114.99 | 3.71 -8 | 241 | 2.56 -5 | 3.102 | 1.11 0 | 2.24 | 3.02 | 1.88 | 698.7 | 7.4 | .41 |
| 113.98 | 4.45 -8 | 231 | 2.95 -5 | 3.020 | 1.41 0 | 2.34 | 2.48 | 1.96 | 712.9 | 7.0 | .48 |
| 112.97 | 5.34 -8 | 223 | 3.42 -5 | 2.948 | 1.76 0 | 2.42 | 2.05 | 2.03 | 726.0 | 6.6 | .64 |
| 112.02 | 6.29 -8 | 218 | 3.94 -5 | 2.886 | 2.16 0 | 2.49 | 1.72 | 2.08 | 738.4 | 6.2 | .75 |
| 111.02 | 7.46 -8 | 214 | 4.59 -5 | 2.824 | 2.65 0 | 2.56 | 1.44 | 2.14 | 752.7 | 5.9 | .75 |
| 109.99 | 8.77 -8 | 214 | 5.38 -5 | 2.773 | 3.17 0 | 2.61 | 1.23 | 2.18 | 766.0 | 5.5 | .53 |
| 109.01 | 1.02 -7 | 215 | 6.25 -5 | 2.728 | 3.72 0 | 2.65 | 1.06 | 2.21 | 777.6 | 5.2 | .50 |
| 108.01 | 1.17 -7 | 216 | 7.29 -5 | 2.683 | 4.35 0 | 2.68 | .92 | 2.24 | 791.0 | 4.9 | .56 |
| 106.99 | 1.35 -7 | 219 | 8.52 -5 | 2.640 | 5.04 0 | 2.71 | .80 | 2.27 | 804.9 | 4.6 | .51 |
| 106.00 | 1.58 -7 | 218 | 9.90 -5 | 2.589 | 6.01 0 | 2.76 | .68 | 2.31 | 817.4 | 4.3 | .63 |
| 104.96 | 1.91 -7 | 212 | 1.16 -4 | 2.522 | 7.52 0 | 2.84 | .56 | 2.37 | 829.8 | 4.1 | .64 |
| 104.01 | 2.29 -7 | 206 | 1.35 -4 | 2.453 | 9.37 0 | 2.92 | .47 | 2.44 | 842.0 | 3.9 | .92 |
| 103.04 | 2.68 -7 | 206 | 1.58 -4 | 2.394 | 1.12 1 | 2.97 | .40 | 2.49 | 855.7 | 3.6 | .76 |
| 101.96 | 3.09 -7 | 211 | 1.87 -4 | 2.343 | 1.28 1 | 2.98 | .35 | 2.49 | 868.8 | 3.4 | .76 |
| | | | | | | | | | | | .26 |

TABLE 3. Computer Output, Typical Firing, Descending Data

| ALTITUDE KM | DENSITY KG/CU.M | TEMP K | PRESSURE MILLIBAR | WINDS M/SEC SOUTH | WEST | TOTAL | CD | RE | MACH | TOTVEL M/S | TOTRV M/S | DELZ KM | XDB VAR |
|---|---|---|---|---|---|---|---|---|---|---|---|---|---|
| 102.04 | 2.62 -7 | 221 | 1.66 -4 | | | | 2.428 | 1.01 1 | 2.82 | 839.9 | | 10.0 | |
| 100.99 | 3.59 -7 | 191 | 1.96 -4 | | | | 2.265 | 1.58 1 | 3.07 | 850.9 | | 10.0 | 1.25 |
| 100.02 | 4.39 -7 | 185 | 2.33 -4 | | | | 2.163 | 2.01 1 | 3.14 | 857.9 | | 10.0 | 1.20 |
| 98.98 | 5.83 -7 | 170 | 2.84 -4 | | | | 1.988 | 2.91 1 | 3.31 | 865.7 | | 10.0 | .97 |
| 98.02 | 6.42 -7 | 184 | 3.39 -4 | | | | 1.964 | 3.03 1 | 3.22 | 873.3 | | 10.0 | .78 |
| 96.99 | 8.08 -7 | 177 | 4.10 -4 | | | | 1.834 | 3.94 1 | 3.29 | 879.2 | | 10.0 | .84 |
| 96.01 | 9.40 -7 | 182 | 4.92 -4 | | | | 1.772 | 4.51 1 | 3.27 | 886.0 | | 10.0 | .71 |
| 94.98 | 1.19 -6 | 175 | 5.96 -4 | | | | 1.667 | 5.96 1 | 3.36 | 892.1 | | 10.0 | .59 |
| 93.99 | 1.51 -6 | 167 | 7.22 -4 | | | | 1.577 | 7.87 1 | 3.45 | 894.7 | | 10.0 | .58 |
| 93.01 | 1.88 -6 | 163 | 8.80 -4 | | | | 1.509 | 1.00 2 | 3.50 | 897.2 | | 10.0 | .61 |
| 92.04 | 2.46 -6 | 153 | 1.08 -3 | | | | 1.420 | 1.39 2 | 3.61 | 896.7 | | 10.0 | .50 |
| 90.97 | 3.09 -6 | 154 | 1.36 -3 | | | | 1.368 | 1.75 2 | 3.60 | 895.8 | | 10.0 | .53 |
| 89.98 | 3.70 -6 | 158 | 1.68 -3 | | | | 1.338 | 2.03 2 | 3.54 | 892.5 | | 10.0 | .55 |
| 89.01 | 4.30 -6 | 166 | 2.05 -3 | | | | 1.322 | 2.26 2 | 3.44 | 886.4 | | 9.4 | 1.07 |
| 87.97 | 5.02 -6 | 174 | 2.51 -3 | | | | 1.307 | 2.50 2 | 3.32 | 877.5 | | 8.8 | 1.23 |
| 87.02 | 5.69 -6 | 183 | 3.00 -3 | | | | 1.297 | 2.67 2 | 3.20 | 867.0 | | 8.4 | 1.26 |
| 85.98 | 6.42 -6 | 195 | 3.60 -3 | | | | 1.290 | 2.81 2 | 3.05 | 853.8 | | 7.9 | 1.21 |
| 84.98 | 7.37 -6 | 201 | 4.26 -3 | | | | 1.276 | 3.09 2 | 2.96 | 840.0 | | 7.4 | 1.19 |
| 83.99 | 8.60 -6 | 203 | 5.01 -3 | | | | 1.261 | 3.49 2 | 2.87 | 821.0 | | 7.0 | .95 |
| 83.01 | 1.03 -5 | 200 | 5.89 -3 | | | | 1.240 | 4.10 2 | 2.81 | 798.7 | | 6.6 | .93 |
| 81.99 | 1.26 -5 | 195 | 7.01 -3 | | | | 1.215 | 4.96 2 | 2.76 | 773.1 | | 6.2 | 1.01 |
| 81.01 | 1.55 -5 | 187 | 8.31 -3 | | | | 1.193 | 6.09 2 | 2.71 | 743.5 | | 5.8 | .64 |
| 80.01 | 1.97 -5 | 177 | 9.99 -3 | | | | 1.169 | 7.67 2 | 2.63 | 701.3 | | 5.5 | .73 |
| 78.99 | 2.41 -5 | 176 | 1.21 -2 | | | | 1.152 | 8.80 2 | 2.45 | 652.2 | | 5.2 | .64 |
| 78.00 | 2.92 -5 | 175 | 1.47 -2 | | | | 1.130 | 9.88 2 | 2.27 | 602.9 | | 4.9 | .53 |
| 76.98 | 3.51 -5 | 176 | 1.78 -2 | | | | 1.110 | 1.06 3 | 2.04 | 542.4 | | 4.6 | .60 |
| 76.02 | 4.24 -5 | 176 | 2.13 -2 | | | | 1.084 | 1.16 3 | 1.84 | 488.3 | | 4.3 | .50 |
| 75.00 | 4.90 -5 | 183 | 2.58 -2 | | | | 1.052 | 1.13 3 | 1.58 | 427.3 | | 4.1 | .79 |
| 74.00 | 5.57 -5 | 192 | 3.08 -2 | | | | 1.018 | 1.08 3 | 1.35 | 373.6 | | 3.8 | .73 |
| 73.00 | 6.20 -5 | 205 | 3.65 -2 | | | | .975 | 1.00 3 | 1.15 | 330.1 | | 3.6 | .74 |
| 72.01 | 6.83 -5 | 217 | 4.26 -2 | | | | .899 | 9.36 2 | .99 | 293.9 | | 3.4 | .52 |
| 70.99 | 8.64 -5 | 202 | 5.01 -2 | | | | .725 | 1.15 3 | .94 | 267.1 | | 3.2 | .86 |
| 70.00 | 1.03 -4 | 200 | 5.91 -2 | -2.0 | 29.4 | 29.5 | .635 | 1.32 3 | .90 | 249.9 | 255.9 | 3.0 | .82 |
| 69.01 | 1.24 -4 | 197 | 6.99 -2 | -24.4 | 1.0 | 24.4 | .576 | 1.45 3 | .82 | 230.6 | 230.9 | 3.0 | 1.19 |
| 68.01 | 1.43 -4 | 201 | 8.27 -2 | 6.6 | -2.4 | 7.0 | .526 | 1.54 3 | .76 | 215.1 | 215.2 | 3.0 | .90 |
| 67.00 | 1.53 -4 | 221 | 9.71 -2 | 3.8 | 8.1 | 8.9 | .504 | 1.49 3 | .71 | 210.6 | 211.9 | 3.0 | .81 |
| 66.01 | 1.69 -4 | 232 | 1.12 -1 | -3.6 | -32.7 | 32.9 | .475 | 1.46 3 | .64 | 194.5 | 195.2 | 3.0 | .67 |
| 65.00 | 1.91 -4 | 236 | 1.30 -1 | 11.3 | -17.5 | 20.9 | .465 | 1.54 3 | .60 | 182.9 | 184.1 | 3.0 | 1.01 |
| 64.00 | 2.19 -4 | 238 | 1.49 -1 | -.9 | 59.1 | 59.1 | .464 | 1.74 3 | .59 | 175.4 | 183.2 | 3.0 | .56 |
| 63.00 | 2.54 -4 | 237 | 1.72 -1 | -7.2 | 44.5 | 45.1 | .456 | 1.84 3 | .54 | 166.0 | 166.9 | 3.0 | .77 |
| 61.99 | 2.77 -4 | 249 | 1.98 -1 | 11.5 | 46.2 | 47.6 | .450 | 1.86 3 | .51 | 160.3 | 160.7 | 3.0 | .31 |
| 61.00 | 3.09 -4 | 254 | 2.26 -1 | -3.5 | 12.5 | 13.0 | .444 | 1.92 3 | .47 | 152.9 | 151.5 | 3.0 | .17 |
| 60.00 | 3.38 -4 | 265 | 2.57 -1 | -6.3 | 16.1 | 17.3 | .441 | 1.90 3 | .43 | 142.8 | 141.4 | 3.0 | .21 |
| 59.00 | 3.81 -4 | 267 | 2.92 -1 | 19.8 | 7.3 | 21.1 | .438 | 2.05 3 | .42 | 136.0 | 136.2 | 3.0 | .16 |
| 57.99 | 4.28 -4 | 269 | 3.31 -1 | 15.8 | -3.1 | 16.1 | .434 | 2.15 3 | .39 | 127.6 | 127.7 | 3.0 | .17 |
| 57.01 | 4.85 -4 | 269 | 3.74 -1 | 18.2 | -.3 | 18.2 | .433 | 2.26 3 | .36 | 119.4 | 118.8 | 3.0 | .29 |
| 56.00 | 5.37 -4 | 274 | 4.24 -1 | 9.6 | -8.4 | 12.8 | .432 | 2.34 3 | .34 | 113.5 | 112.8 | 3.0 | .28 |
| 55.00 | 5.83 -4 | 285 | 4.78 -1 | 7.8 | -3.0 | 8.3 | .432 | 2.35 3 | .32 | 108.2 | 107.6 | 3.0 | .32 |
| 54.00 | 6.46 -4 | 289 | 5.37 -1 | -.4 | -1.7 | 1.8 | .431 | 2.44 3 | .30 | 101.8 | 101.8 | 3.0 | .32 |
| 53.00 | 7.22 -4 | 291 | 6.03 -1 | -6.8 | -7.3 | 9.9 | .430 | 2.58 3 | .28 | 96.9 | 97.1 | 3.0 | .31 |
| 52.00 | 8.12 -4 | 291 | 6.77 -1 | -1.8 | -16.9 | 17.0 | .429 | 2.74 3 | .27 | 91.9 | 91.5 | 3.0 | .32 |
| 51.00 | 9.34 -4 | 284 | 7.61 -1 | 6.1 | -20.9 | 21.7 | .427 | 3.00 3 | .25 | 87.3 | 85.7 | 3.0 | .39 |
| 50.00 | 1.06 -3 | 281 | 8.57 -1 | 6.2 | -25.7 | 26.4 | .427 | 3.14 3 | .23 | 81.4 | 78.0 | 3.0 | .36 |
| 49.00 | 1.21 -3 | 279 | 9.68 -1 | .3 | -28.2 | 28.2 | .427 | 3.44 3 | .22 | 78.8 | 74.5 | 3.0 | .25 |
| 48.00 | 1.36 -3 | 279 | 1.09 0 | -4.5 | -22.3 | 22.7 | .426 | 3.62 3 | .21 | 73.9 | 69.8 | 3.0 | .18 |
| 47.00 | 1.52 -3 | 282 | 1.23 0 | -4.0 | -19.7 | 20.1 | .426 | 3.75 3 | .19 | 68.7 | 65.3 | 3.0 | .22 |
| 46.00 | 1.75 -3 | 276 | 1.39 0 | 1.5 | -19.2 | 19.2 | .427 | 4.22 3 | .19 | 65.5 | 62.6 | 3.0 | .29 |
| 45.00 | 1.93 -3 | 282 | 1.57 0 | 4.8 | -22.2 | 22.7 | .426 | 4.10 3 | .17 | 60.2 | 56.0 | 3.0 | .49 |
| 44.00 | 2.23 -3 | 276 | 1.77 0 | 2.4 | -19.1 | 19.3 | .429 | 4.81 3 | .17 | 59.4 | 56.1 | 3.0 | .84 |
| 43.00 | 2.43 -3 | 285 | 1.99 0 | 1.2 | -21.8 | 21.9 | .428 | 4.54 3 | .15 | 54.2 | 49.8 | 3.0 | .62 |
| 42.00 | 2.83 -3 | 277 | 2.25 0 | -.2 | -20.8 | 20.8 | .432 | 5.33 3 | .15 | 53.3 | 49.2 | 3.0 | .54 |
| 41.00 | 3.17 -3 | 278 | 2.54 0 | 6.7 | -23.7 | 24.7 | .432 | 5.37 3 | .13 | 50.2 | 44.3 | 3.0 | 1.09 |
| 40.00 | 3.76 -3 | 266 | 2.88 0 | 7.7 | -22.6 | 23.9 | .436 | 6.20 3 | .13 | 48.0 | 41.7 | 3.0 | .87 |
| 39.00 | 4.37 -3 | 261 | 3.27 0 | 2.9 | -23.5 | 23.7 | .438 | 6.53 3 | .11 | 44.3 | 37.2 | 3.0 | .38 |
| 38.00 | 5.15 -3 | 253 | 3.73 0 | 1.3 | -20.9 | 20.9 | .443 | 7.39 3 | .11 | 40.9 | 34.8 | 3.0 | .68 |
| 37.00 | 6.19 -3 | 241 | 4.28 0 | 6.1 | -23.1 | 23.9 | .449 | 8.46 3 | .10 | 39.4 | 32.0 | 3.0 | .82 |
| 36.00 | 7.07 -3 | 242 | 4.92 0 | 4.0 | -31.9 | 32.2 | .448 | 8.35 3 | .09 | 42.0 | 27.6 | 3.0 | .81 |
| 35.00 | 8.13 -3 | 242 | 5.65 0 | -5.8 | -33.2 | 33.7 | .456 | 9.82 3 | .09 | 43.8 | 28.3 | 3.0 | 1.09 |
| 34.00 | 9.37 -3 | 242 | 6.51 0 | -8.0 | -36.3 | 37.2 | .457 | 1.01 4 | .08 | 44.8 | 25.1 | 3.0 | .80 |
| 33.00 | 1.16 -2 | 227 | 7.52 0 | -1.8 | -41.9 | 42.0 | .463 | 1.15 4 | .07 | 47.2 | 22.1 | 3.0 | 1.01 |
| 32.00 | 1.41 -2 | 217 | 8.76 0 | 4.1 | -43.4 | 43.6 | .469 | 1.32 4 | .07 | 48.0 | 20.0 | 3.0 | 1.01 |

TABLE 4. Drag Coefficient Used When Mach Number Exceeds 2.5

| Re | $C_{D_R}$ | Re | $C_{D_R}$ |
|---|---|---|---|
| 50 | 1.73 | 3000 | 1.050 |
| 70 | 1.61 | 4000 | 1.030 |
| 100 | 1.51 | 5000 | 1.017 |
| 150 | 1.40 | 6000 | 1.006 |
| 200 | 1.34 | 7000 | .999 |
| 300 | 1.28 | 8000 | .990 |
| 500 | 1.214 | 9000 | .985 |
| 700 | 1.178 | 10000 | .980 |
| 900 | 1.153 | 15000 | .965 |
| 1000 | 1.143 | 20000 | .950 |
| 1500 | 1.107 | 30000 | .950 |
| 2000 | 1.080 | 40000 | .950 |

For small Reynolds number an extrapolation is used.

$$C_{D_R} = 2.5 - .023267\ Re + .00015734\ Re^2 \qquad Re < 50$$

TABLE 5. Drag Coefficient Used When Mach Number is Less Than 2.5

| Reynolds Number ↓ \ Mach Number → | 0 | .390 | .485 | .530 | .620 | .685 | .750 | .800 | .850 | .900 | 1.0 | 1.2 | 1.4 | 1.6 | 1.8 | 2.0 | 2.5 |
|---|---|---|---|---|---|---|---|---|---|---|---|---|---|---|---|---|---|
| 200 | | | | | | | | | | | 1.107 | 1.193 | 1.232 | 1.264 | 1.290 | 1.310 | 1.340 |
| 300 | | | | | | | | | | | 1.047 | 1.133 | 1.172 | 1.204 | 1.230 | 1.250 | 1.280 |
| 500 | | | | | | | | | | | .981 | 1.067 | 1.106 | 1.138 | 1.164 | 1.184 | 1.214 |
| 700 | | | | | | | | | | | .945 | 1.031 | 1.070 | 1.102 | 1.128 | 1.148 | 1.178 |
| 900 | .410 | .410 | .411 | .428 | .447 | .480 | .506 | .528 | .565 | .598 | .920 | 1.006 | 1.045 | 1.077 | 1.103 | 1.123 | 1.153 |
| 1000 | .418 | .418 | .418 | .437 | .453 | .486 | .511 | .538 | .574 | .608 | .912 | .996 | 1.035 | 1.067 | 1.093 | 1.113 | 1.143 |
| 1500 | .443 | .443 | .442 | .454 | .468 | .493 | .520 | .561 | .600 | .640 | .885 | .960 | .999 | 1.031 | 1.057 | 1.077 | 1.107 |
| 2000 | .435 | .435 | .446 | .454 | .468 | .489 | .516 | .568 | .611 | .656 | .863 | .933 | .972 | 1.004 | 1.030 | 1.050 | 1.080 |
| 3000 | .427 | .427 | .440 | .450 | .463 | .486 | .516 | .570 | .619 | .668 | .838 | .903 | .942 | .974 | 1.000 | 1.020 | 1.050 |
| 4000 | .426 | .426 | .442 | .450 | .463 | .486 | .516 | .572 | .623 | .674 | .882 | .883 | .922 | .954 | .980 | 1.000 | 1.030 |
| 5000 | .430 | .430 | .442 | .450 | .463 | .486 | .516 | .577 | .626 | .678 | .811 | .870 | .909 | .941 | .967 | .987 | 1.017 |
| 6000 | .435 | .435 | .442 | .450 | .463 | .486 | .516 | .583 | .629 | .680 | .801 | .859 | .898 | .930 | .956 | .976 | 1.006 |
| 7000 | .441 | .441 | .441 | .450 | .463 | .486 | .516 | .587 | .633 | .683 | .796 | .852 | .891 | .923 | .949 | .969 | .999 |
| 8000 | .446 | .446 | .446 | .450 | .463 | .486 | .516 | .588 | .635 | .684 | .788 | .843 | .882 | .914 | .940 | .960 | .990 |
| 9000 | .452 | .452 | .452 | .452 | .463 | .486 | .516 | .590 | .637 | .687 | .784 | .838 | .877 | .909 | .935 | .955 | .985 |
| 10000 | .457 | .457 | .457 | .457 | .463 | .486 | .516 | .592 | .639 | .689 | .780 | .833 | .872 | .904 | .930 | .950 | .980 |
| 15000 | .474 | .474 | .474 | .474 | .474 | .486 | .516 | .597 | .647 | .695 | .768 | .818 | .857 | .889 | .915 | .935 | .965 |
| 20000 | .482 | .482 | .482 | .482 | .482 | .486 | .516 | .602 | .652 | .700 | .755 | .803 | .842 | .874 | .900 | .920 | .950 |
| 30000 | .491 | .491 | .491 | .491 | .491 | .486 | .516 | .608 | .659 | .708 | .755 | .803 | .842 | .874 | .900 | .920 | .950 |
| 40000 | .494 | .494 | .494 | .494 | .494 | .486 | .516 | .612 | .665 | .713 | .757 | .803 | .842 | .874 | .900 | .920 | .950 |

# LIST OF FIGURES

Figure 1. The Tradex radar.

Figure 2. The Nike-Cajun rocket.

Figure 3. Three-sphere payloads.

Figure 4. Instrumentation section and Raymond timer.

Figure 5. Isopentane capsule and inertia release mechanism.

Figure 6. Typical trajectory, 20 June 1963 sounding. Sphere 1 apogee at 186 sec; Cajun apogee at 209 sec; and sphere deflation at 17.5 min, 31 km.

Figure 7. Radar coordinates.

Figure 8. Geocentric triangle.

Figure 9. Altitude band used when retrieving derivatives.

Figure 10. Results of Sounding Number 2.

Figure 11. Results of Sounding Number 3.

Figure 12. Results of Sounding Number 4.

Figure 13. Results of Sounding Number 5.

Figure 14. Results of Sounding Number 6.

Figure 15. Results of Sounding Number 7.

Figure 16. Results of Sounding Number 8.

Figure 17. Results of Sounding Number 11.

Figure 18. Results of Sounding Number 12.

Figure 19. Results of Sounding Number 13.

Figure 20. Results of Sounding Number 14.

LIST OF FIGURES (Concluded)

Figure 21. Results of Sounding Number 15.

Figure 22. Results of Sounding Number 16.

Figure 23. Day-night pair of soundings at Kwajalein.

Figure 24. Results of Soundings of June 1963 and 1964 at Kwajalein.

Figure 25. Summary of thirteen Kwajalein soundings.

Figure 26. Summary of thirteen Kwajalein soundings, wind profiles.

Figure 1. The Tradex radar.

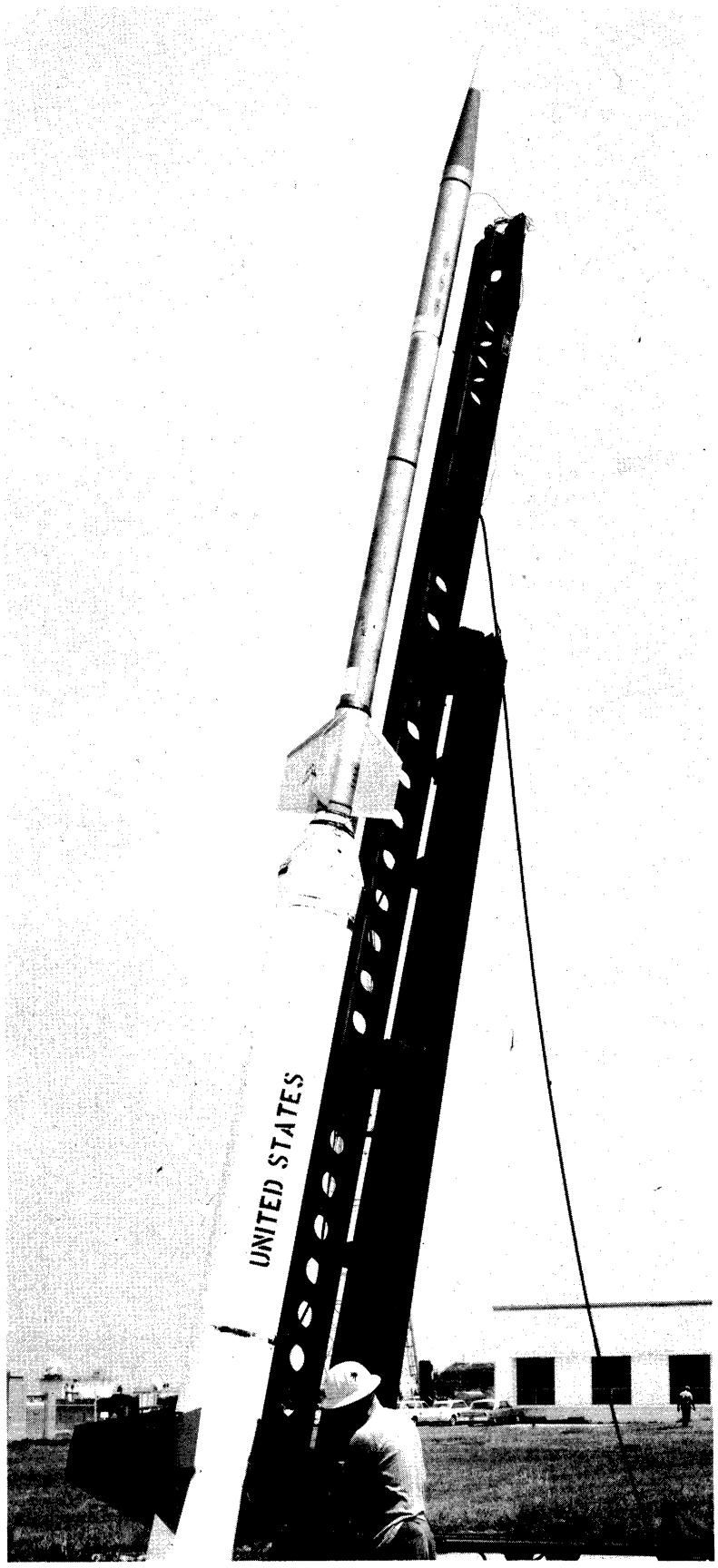


Figure 2. The Nike-Cajun rocket.

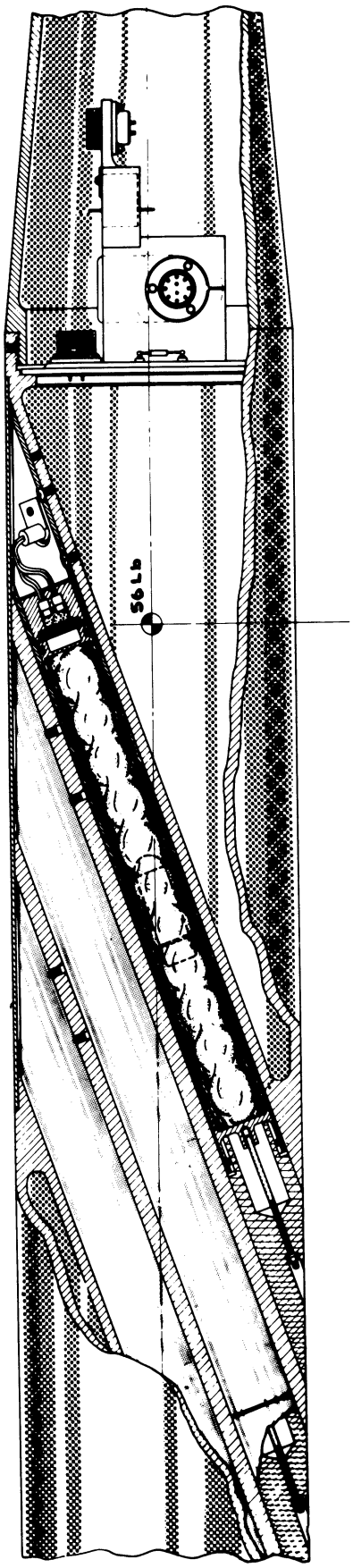


Figure 3. Three-sphere payloads.

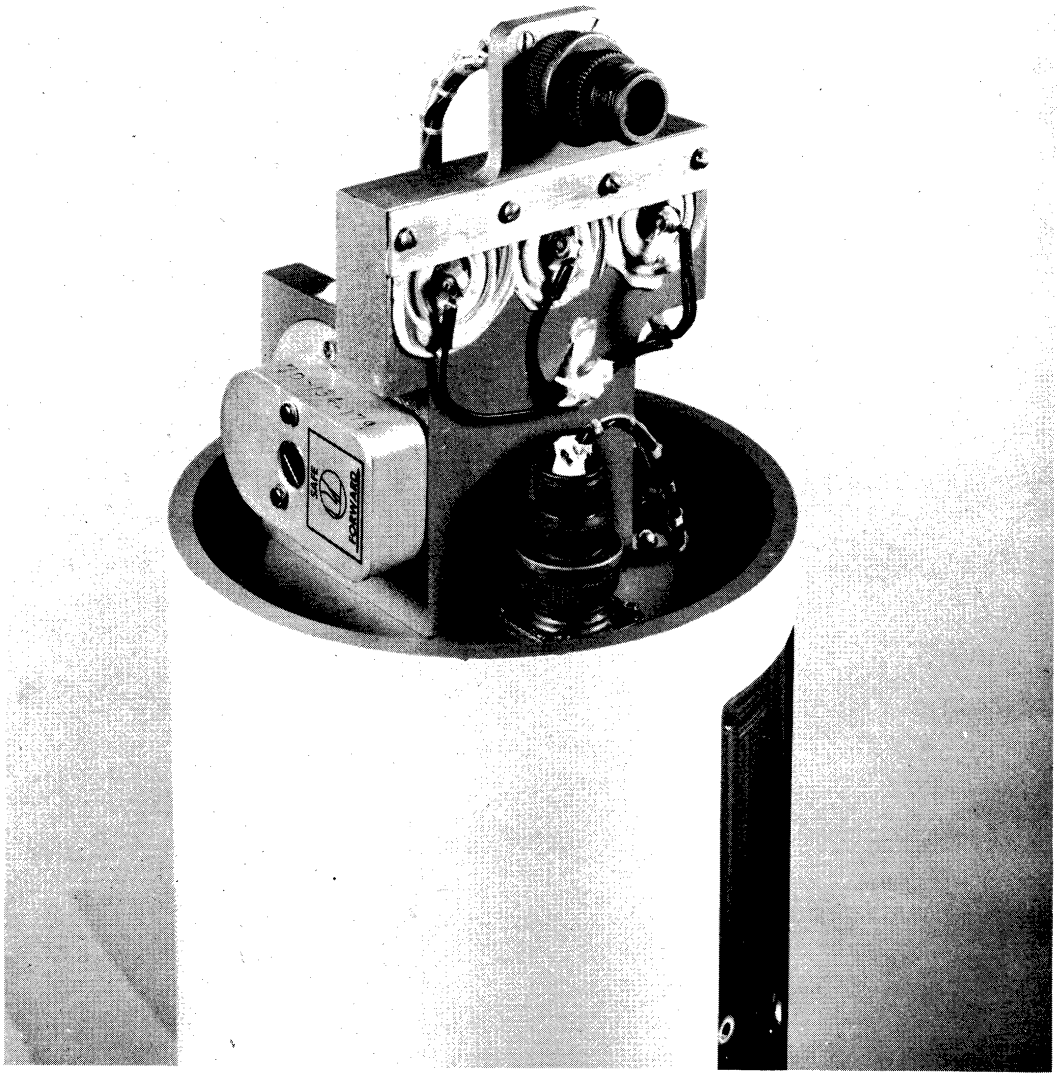

Figure 4. Instrumentation section and Raymond timer.

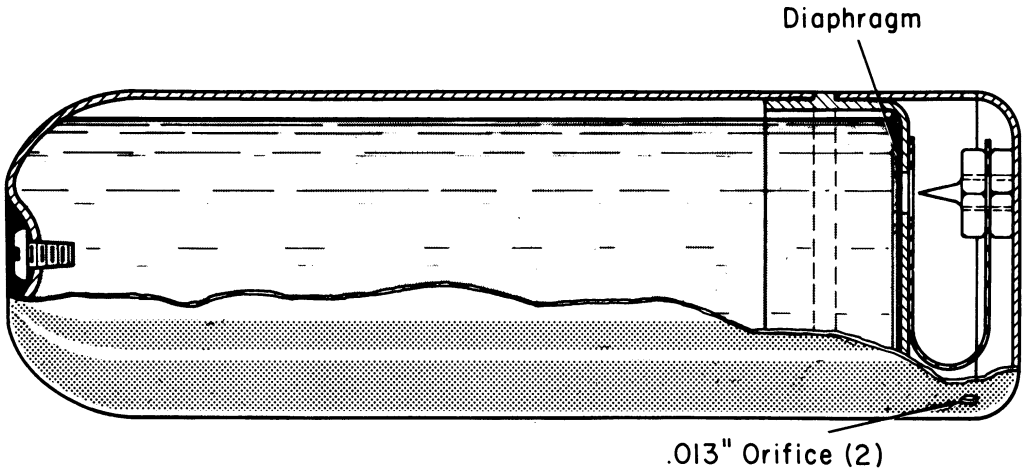


Figure 5. Isopentane capsule and inertia release mechanism.

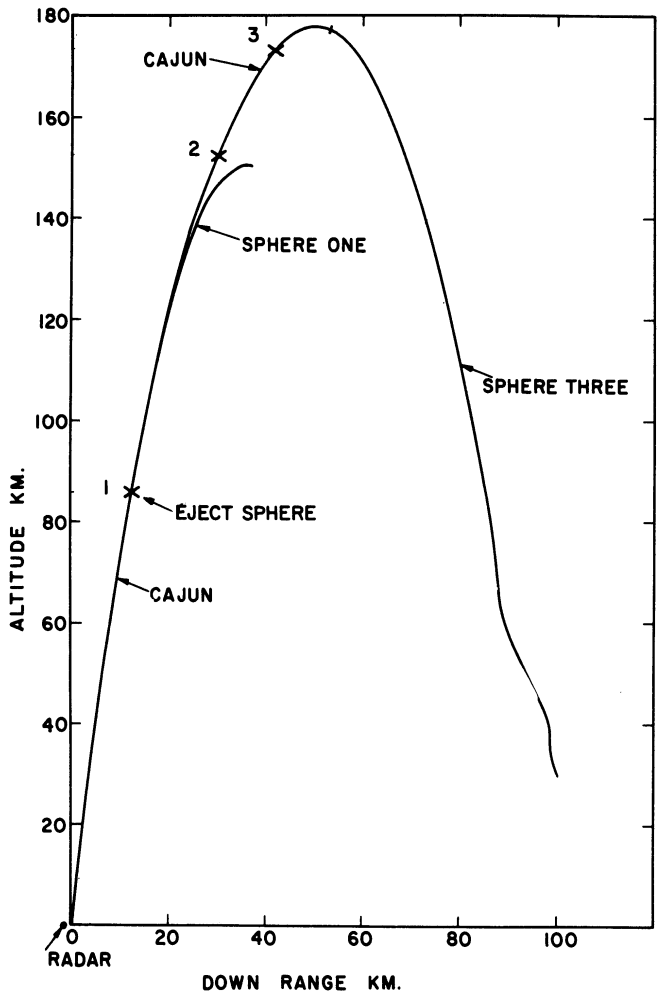


Figure 6. Typical trajectory, 20 June 1963 sounding. Sphere 1 apogee at 186 sec; Cajun apogee at 209 sec; and sphere deflation at 17.5 min, 31 km.

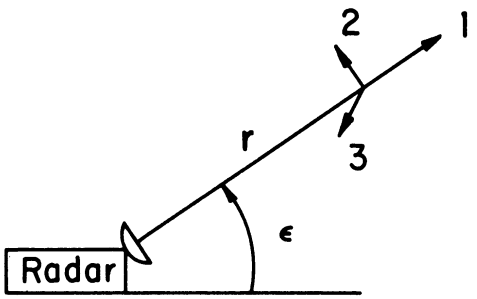


1 r = range
2 ϵ = elevation angle
3 α = azimuth angle

Figure 7. Radar coordinates.

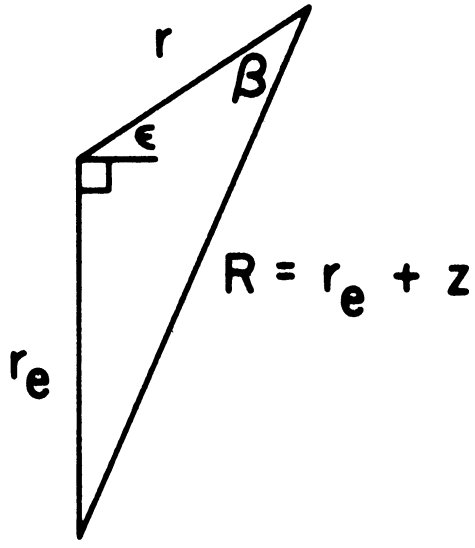


Figure 8. Geocentric triangle.

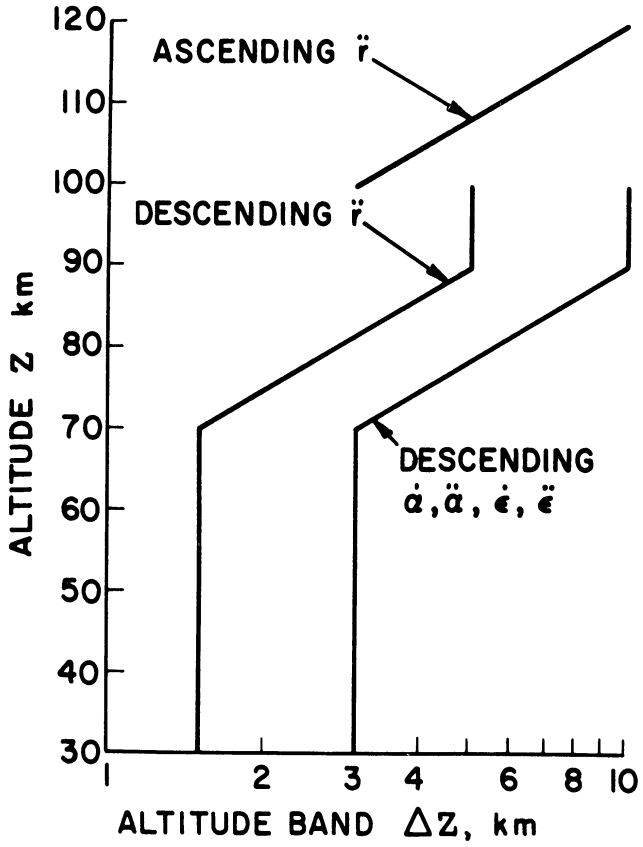


Figure 9. Altitude band used when retrieving derivatives.

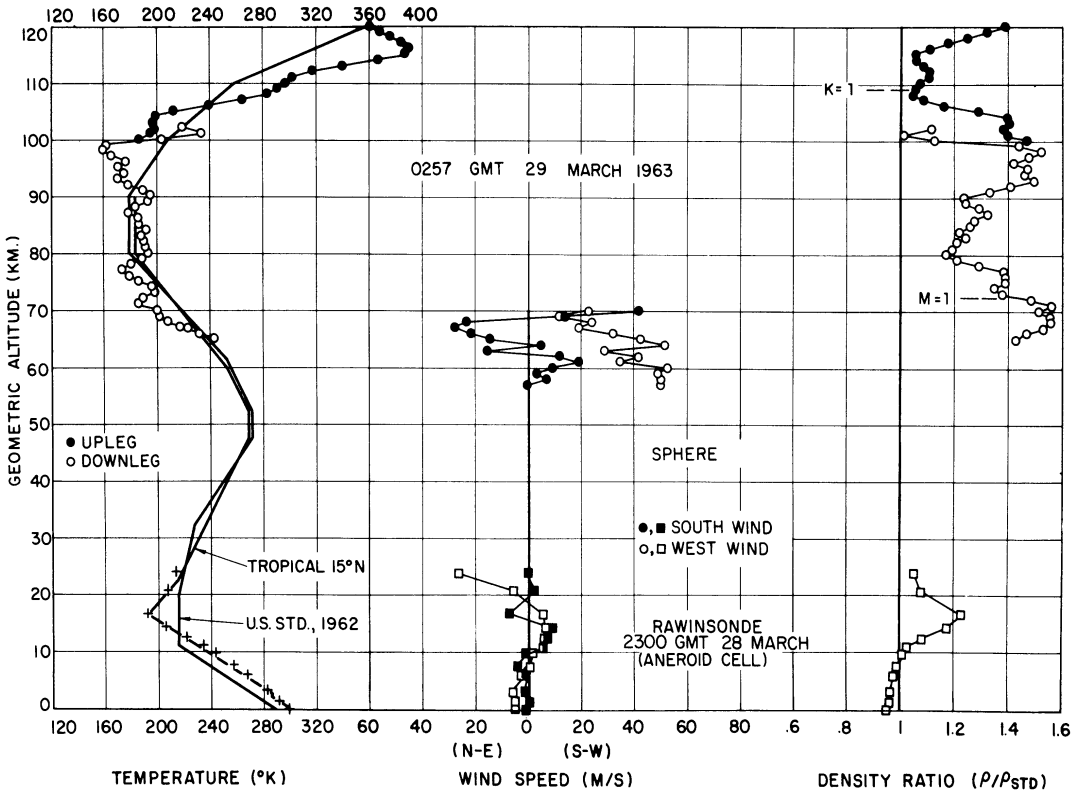


Figure 10. Results of Sounding Number 2.

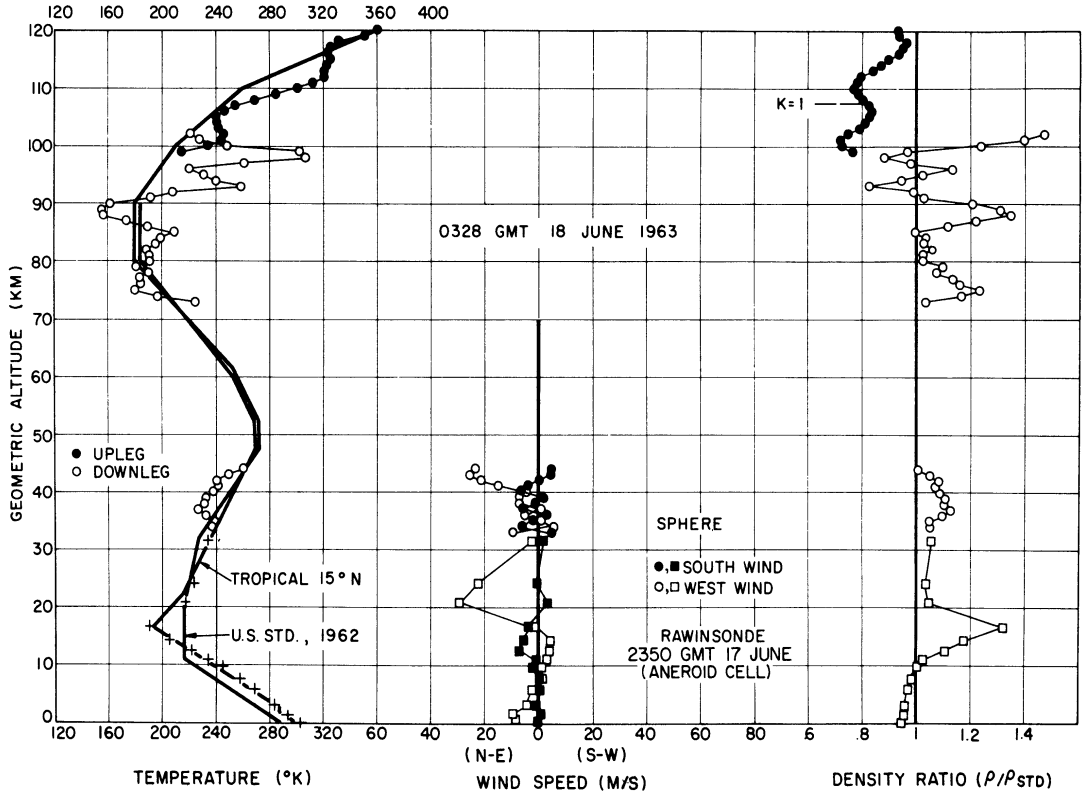


Figure 11. Results of Sounding Number 3.

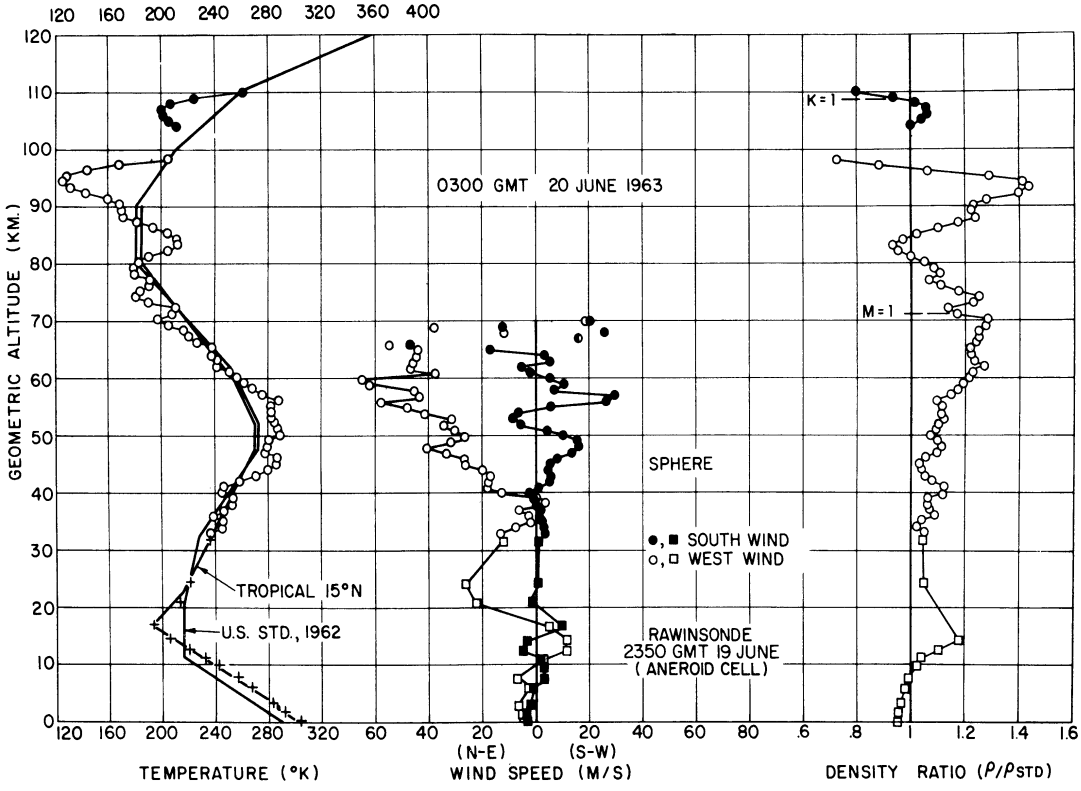


Figure 12. Results of Sounding Number 4.

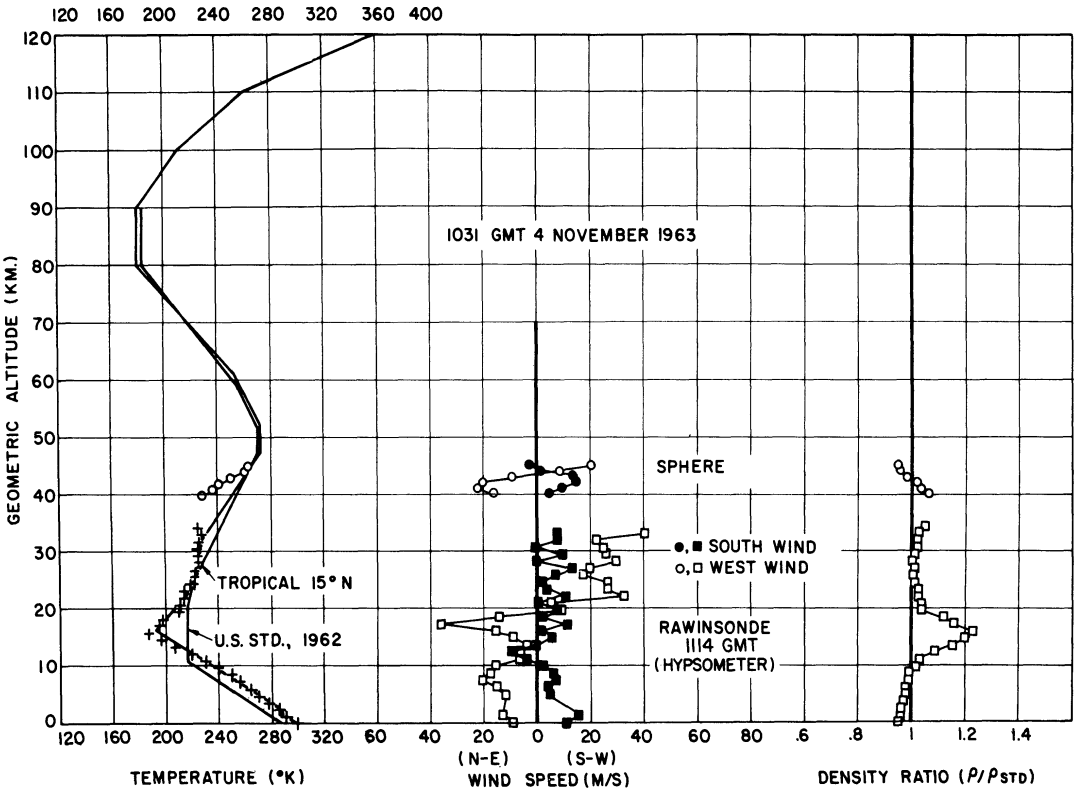


Figure 13. Results of Sounding Number 5.

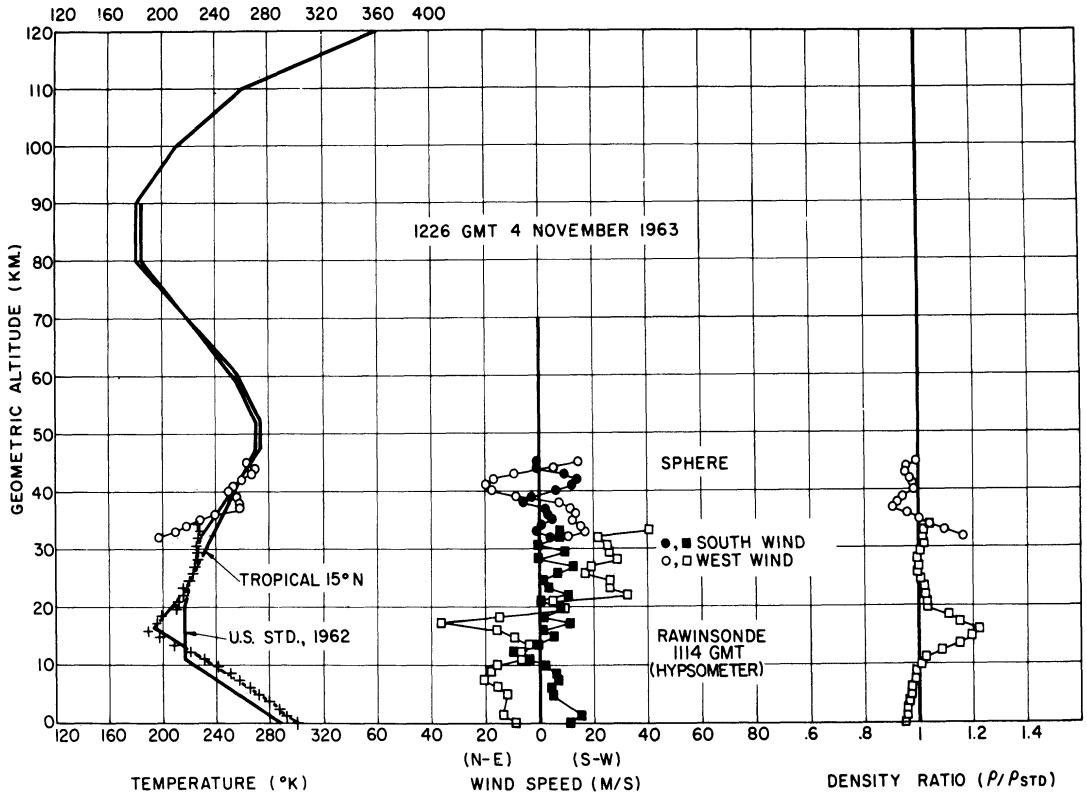


Figure 14. Results of Sounding Number 6.

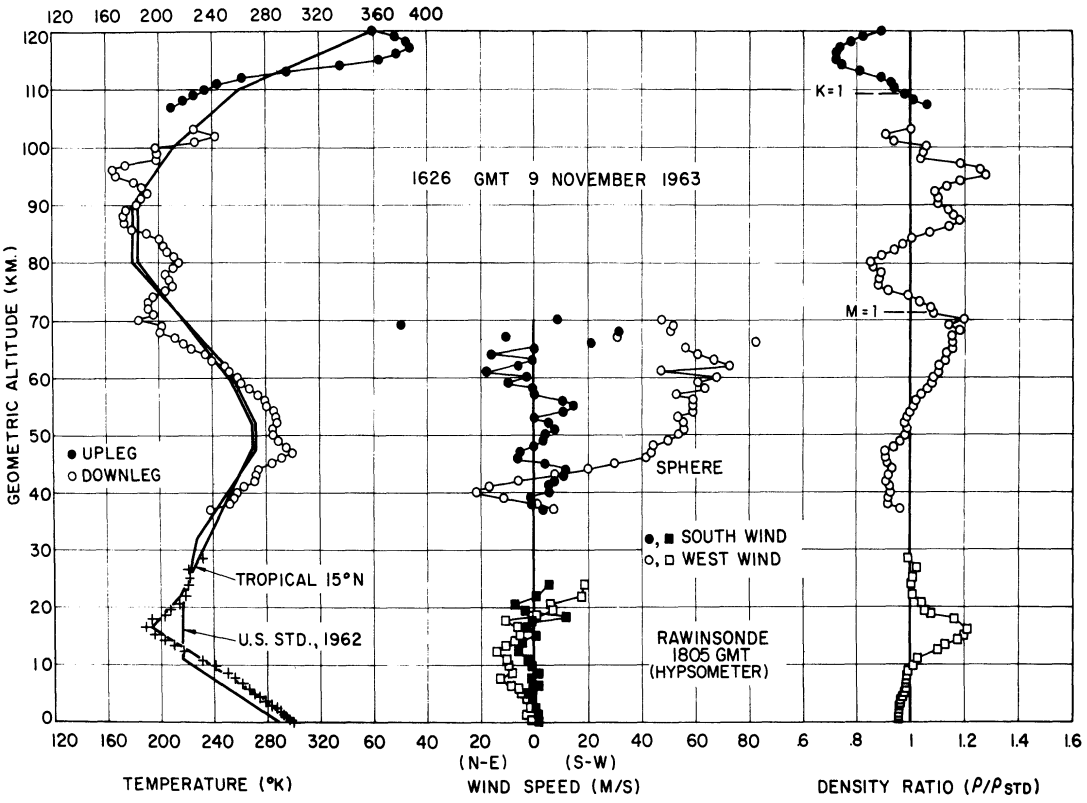


Figure 15. Results of Sounding Number 7.

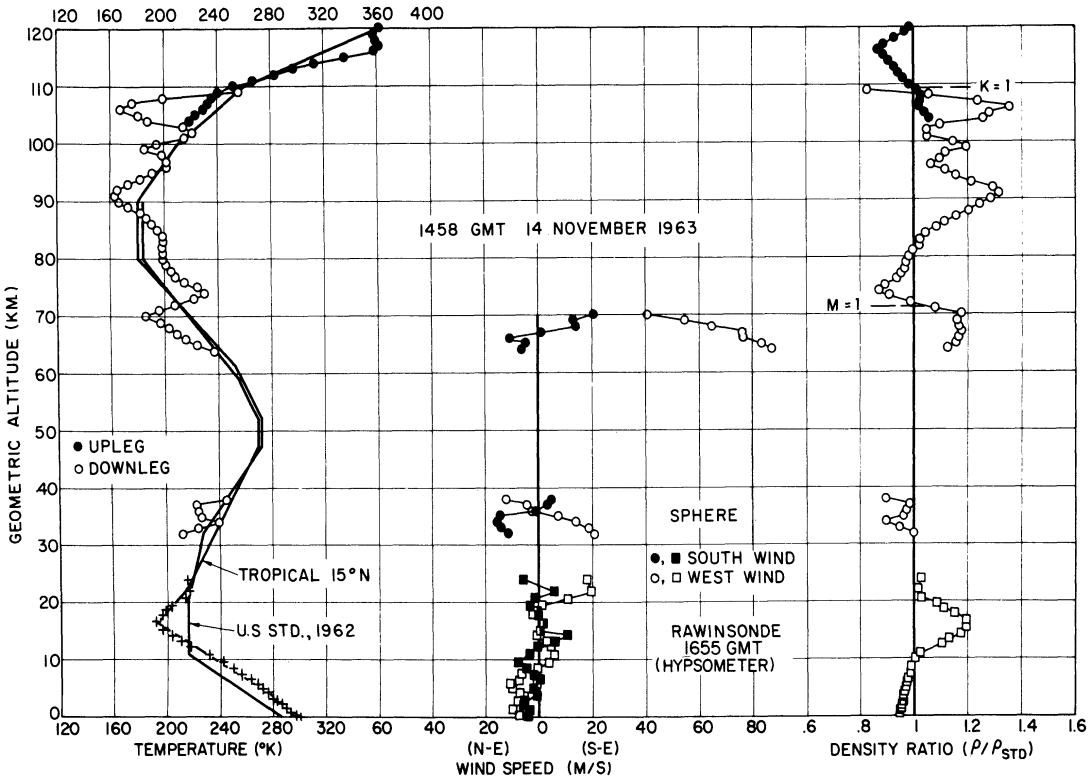


Figure 16. Results of Sounding Number 8.

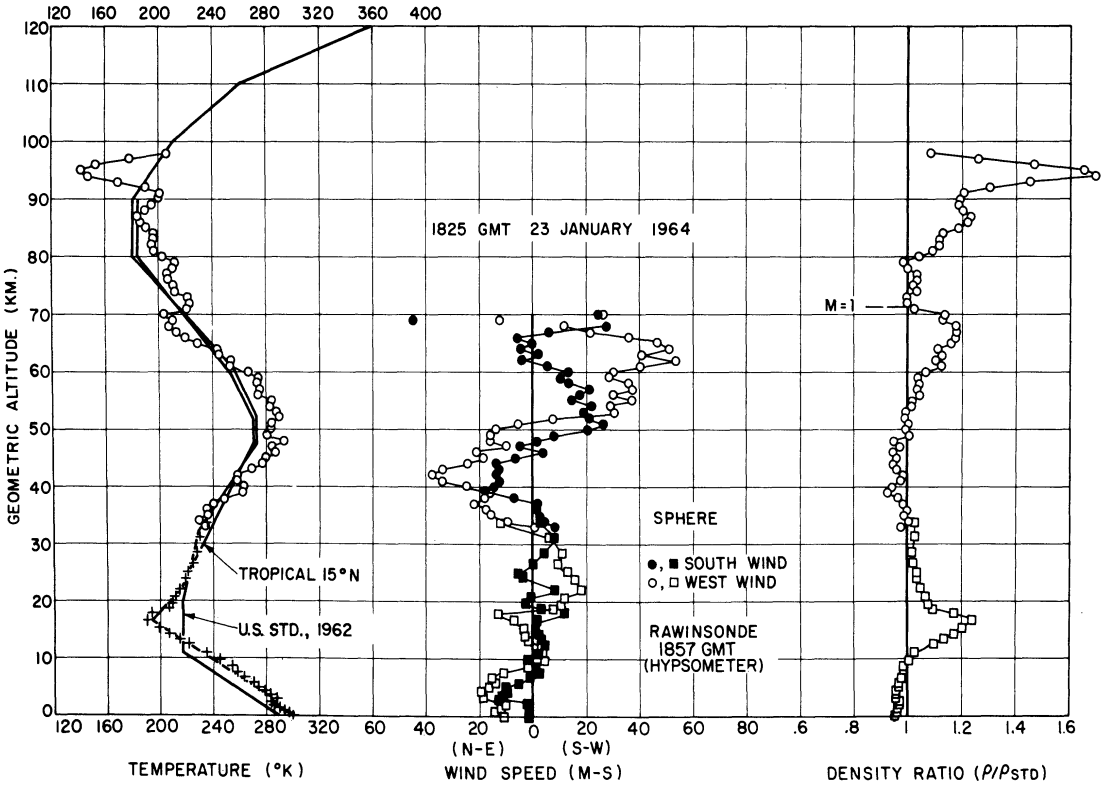


Figure 17. Results of Sounding Number 11.

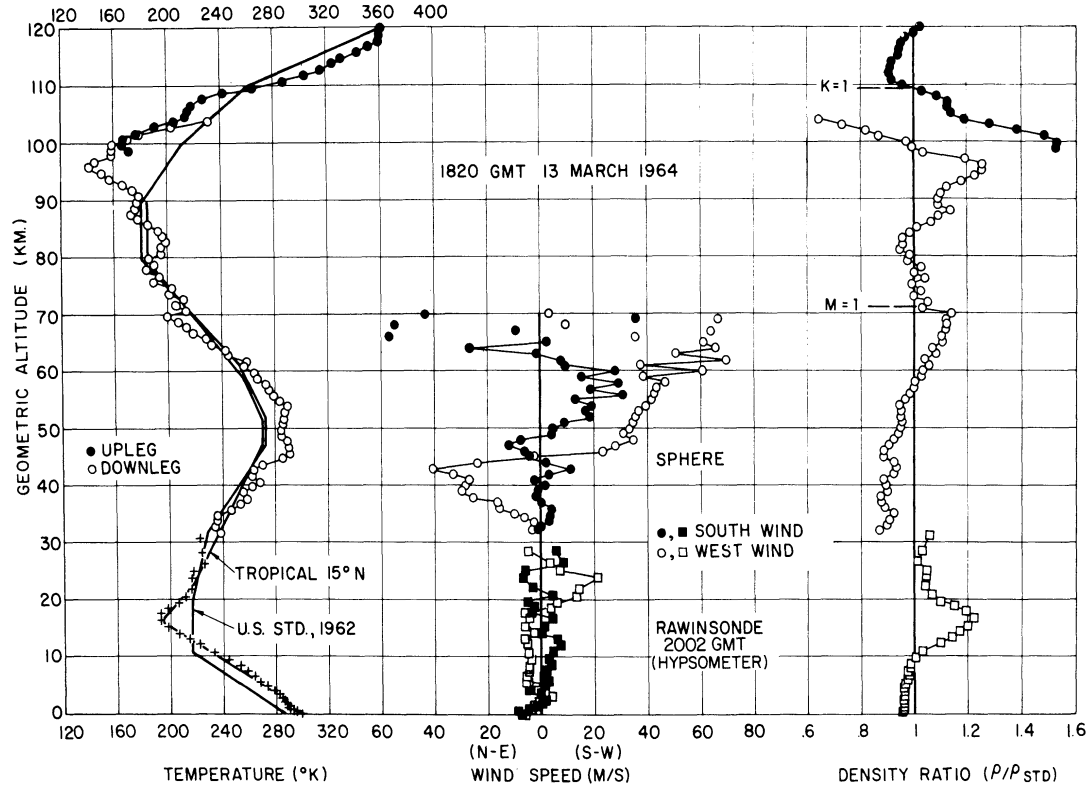


Figure 18. Results of Sounding Number 12.

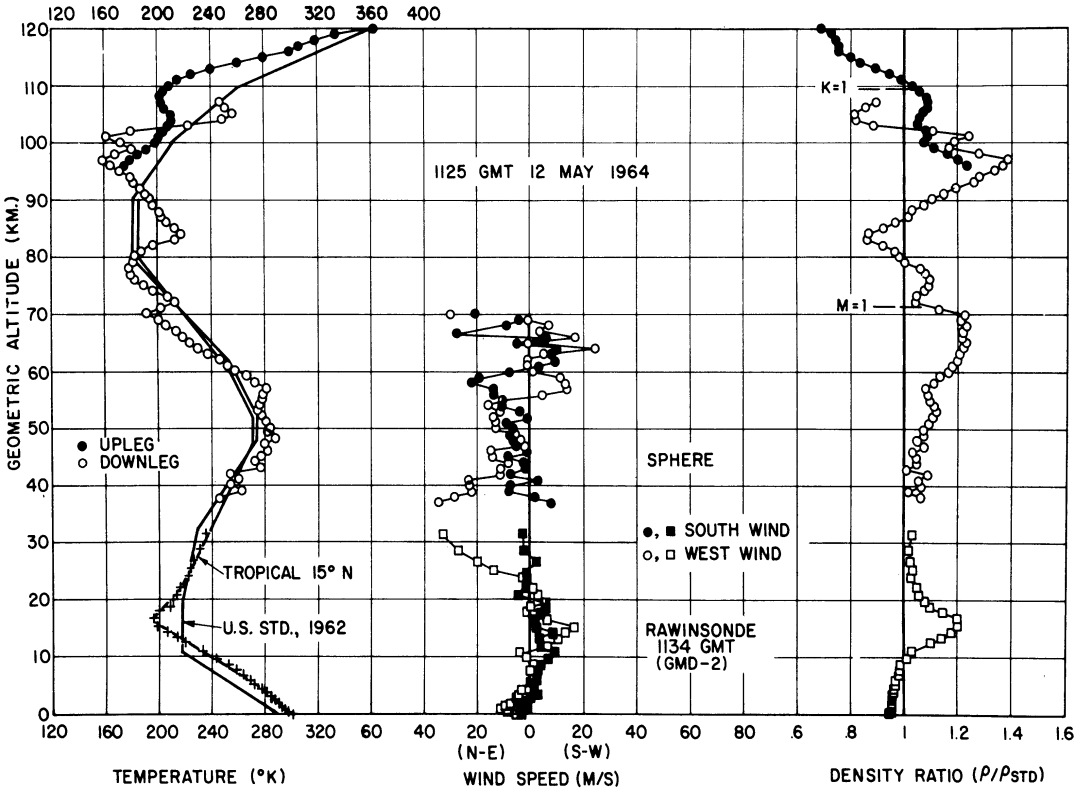


Figure 19. Results of Sounding Number 13.

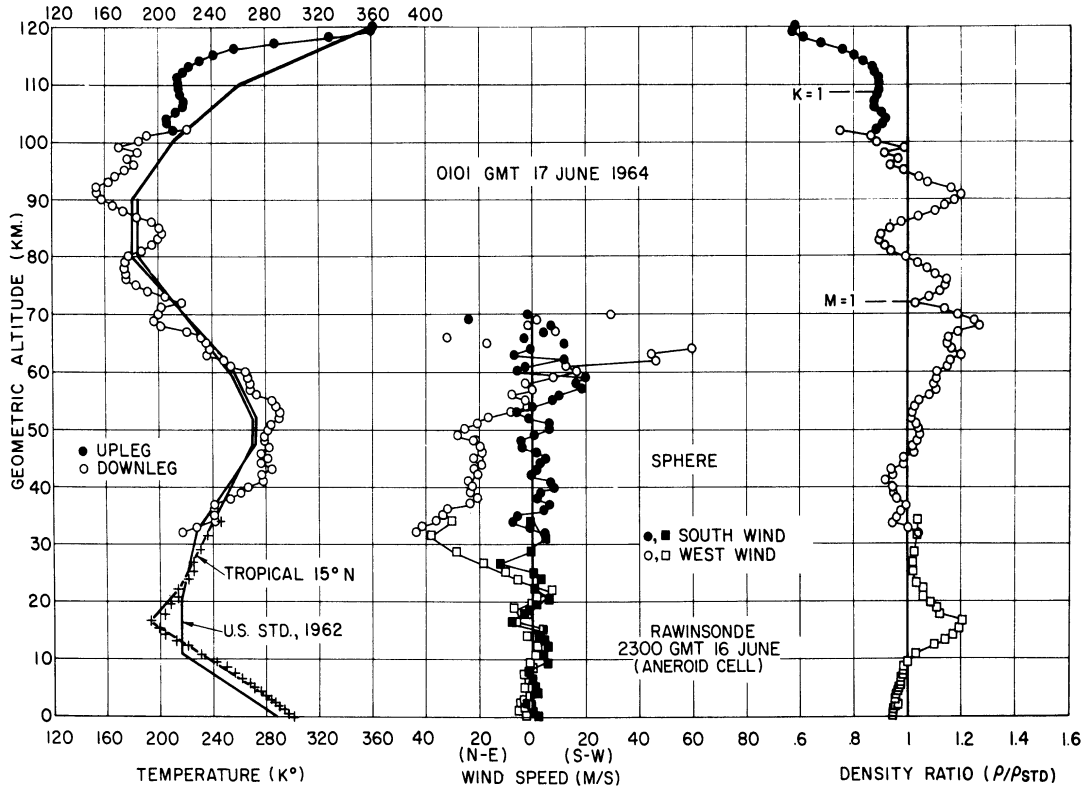


Figure 20. Results of Sounding Number 14.

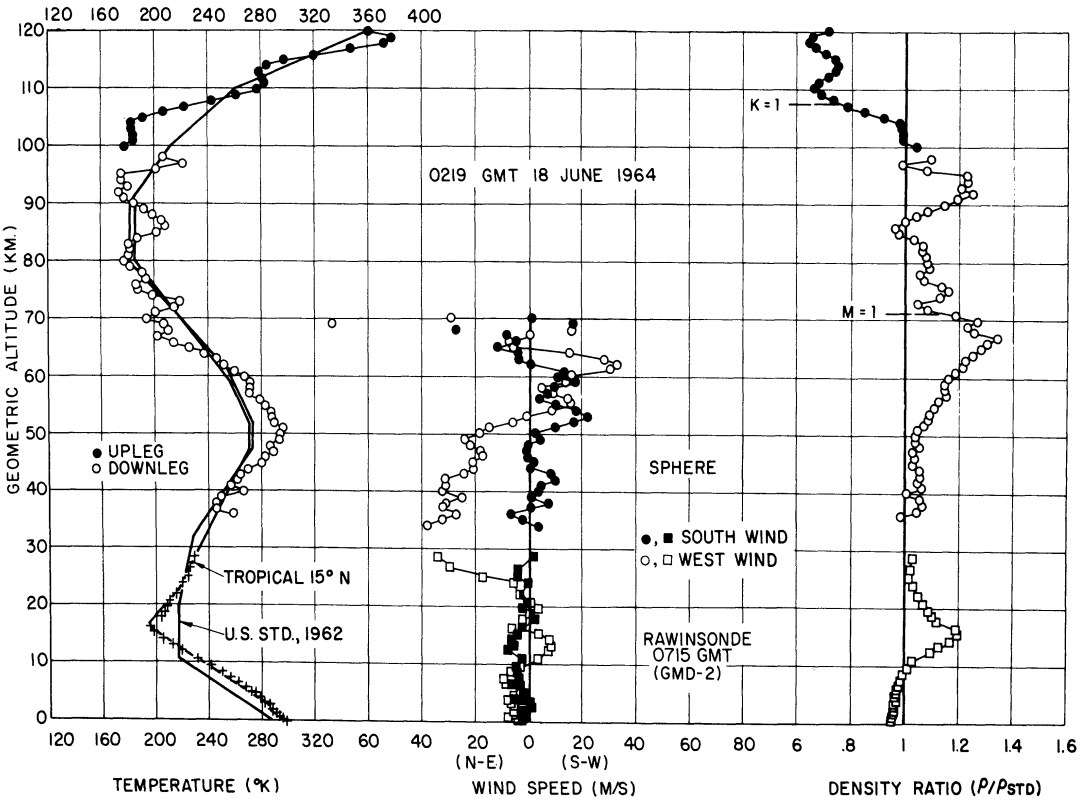


Figure 21. Results of Sounding Number 15.

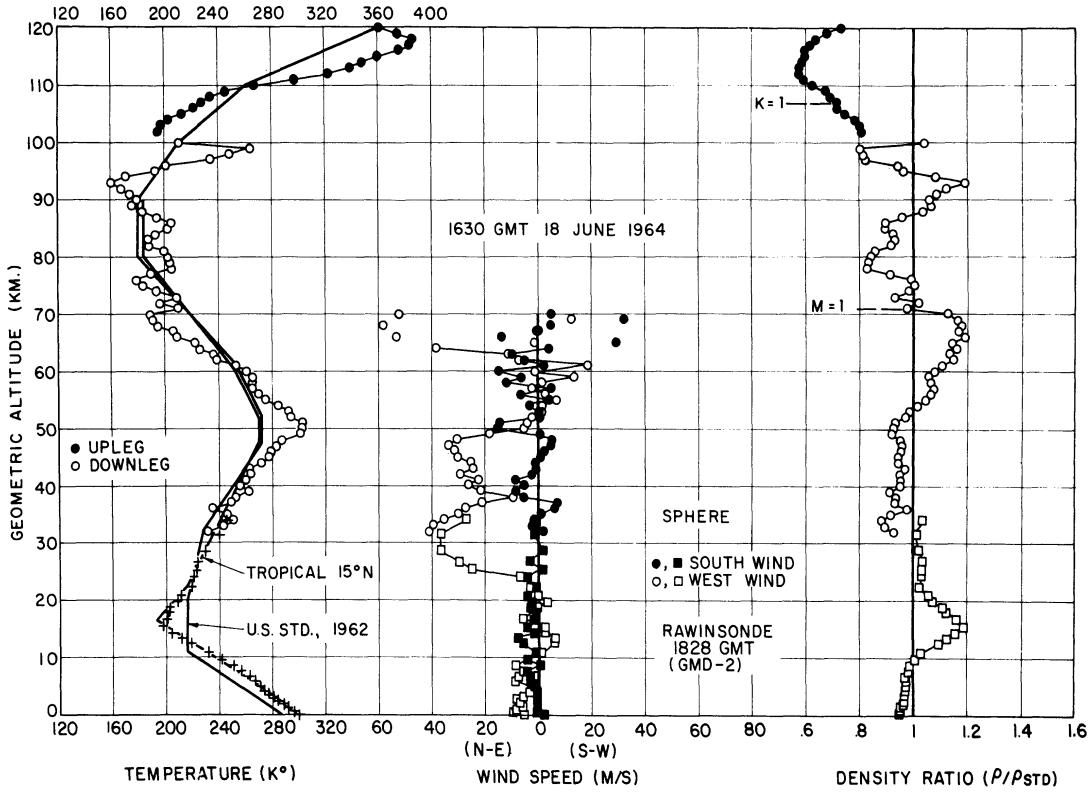


Figure 22. Results of Sounding Number 16.

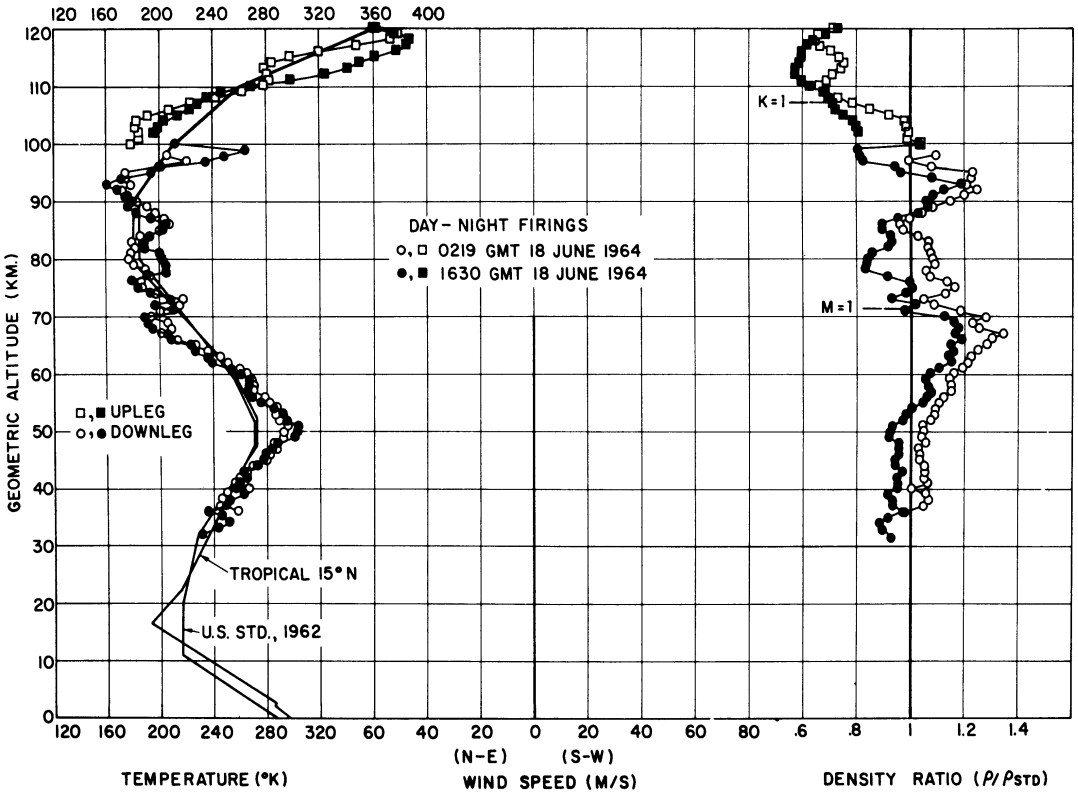


Figure 23. Day-night pair of soundings at Kwajalein.

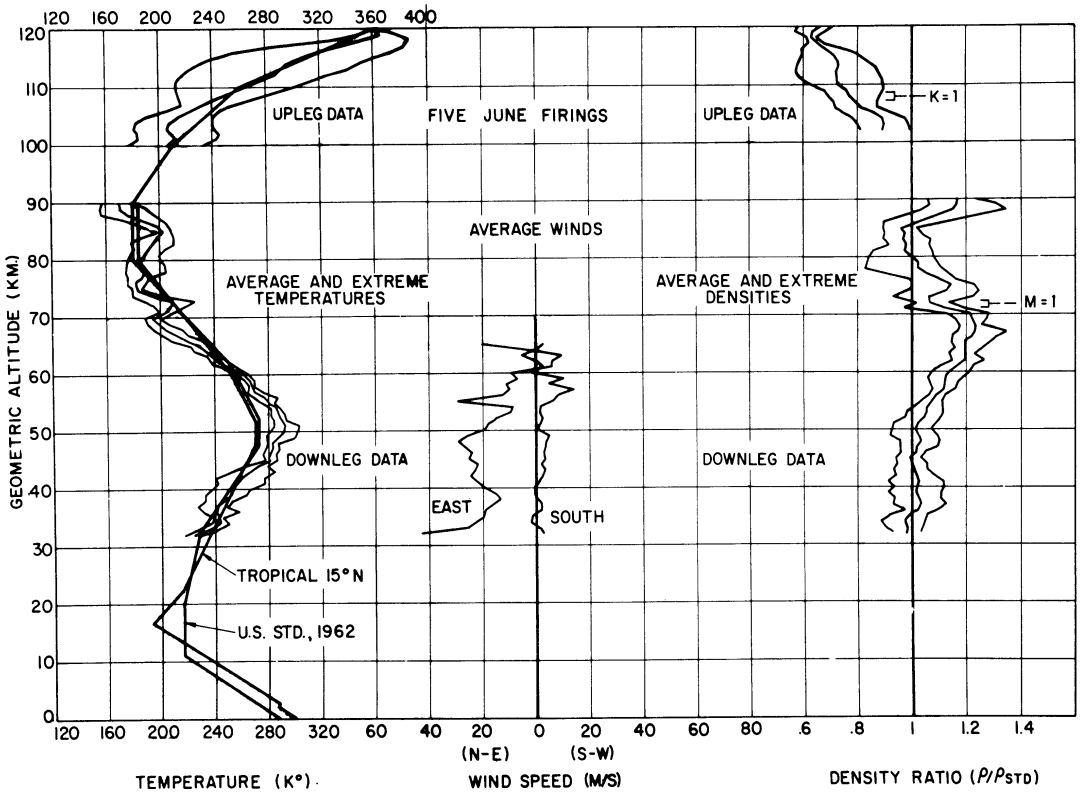


Figure 24. Results of Soundings of June 1963 and 1964 at Kwajalein.

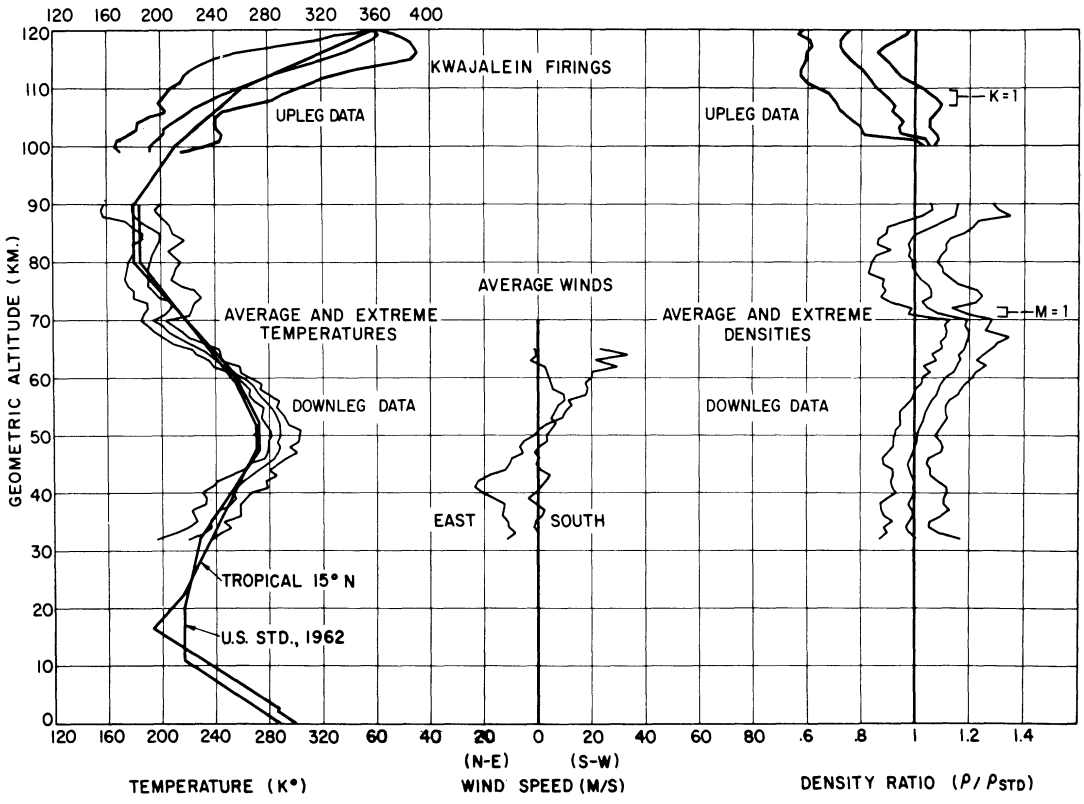


Figure 25. Summary of thirteen Kwajalein soundings.

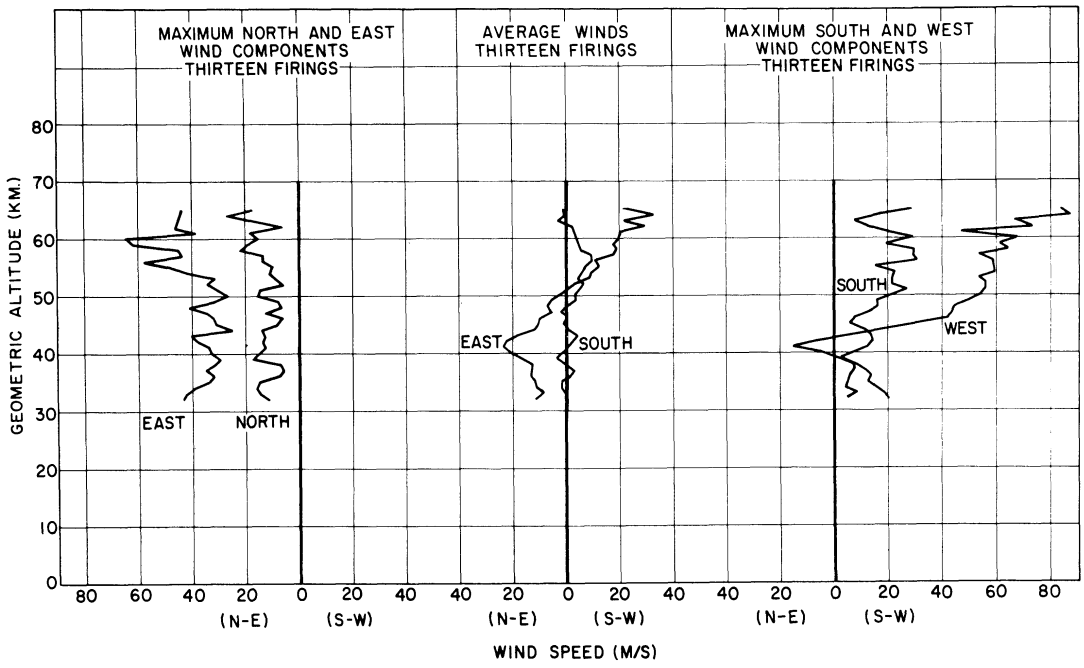


Figure 26. Summary of thirteen Kwajalein soundings, wind profiles.